Six-DOF Motion Response and Manoeuvring Simulation of an Underwater Vehicle

by

Howan Kim

National Centre for Maritime Engineering and Hydrodynamics
Australian Maritime College

Submitted in fulfilment of the requirements for the degree of Doctor of Philosophy
University of Tasmania

September 2017

[Page intentionally left blank]

DECLARATIONS

Authority of Access

The publishers of the papers comprising Chapters 2 – 5 hold the copyright for that content, and access to the material should be sought from the respective journals. The remaining non-published content of this thesis may be made available for loan and limited copying and communication in accordance with the Copyright Act 1968.

Declaration of Originality

This thesis contains no material which has been accepted for a degree or diploma by the University or any other institution, except by way of background information and duly acknowledged in the thesis, and to the best of my knowledge and belief no material previously published or written by another person except where due acknowledgement is made in the text of the thesis, nor does the thesis contain any material that infringes copyright.

Signed: Date: 13 September 2017

Howan Kim

Statement of Published Work Contained in Thesis

The publishers of the papers comprising Chapters 2 and 5 hold the copyright for that content, and access to the material should be sought from the respective journals and conference proceedings. The remaining non published content of the thesis, Chapter 3, is submitted and under review, and may be made available for loan and limited copying and communication in accordance with the Copyright Act 1968.

Statement of Co-Authorship

The following people and institutions contributed to the publication of work undertaken as part of this thesis:

- *Howan Kim, University of Tasmania* = **Candidate**
- *Professor Dev Ranmuthugala, Defence Science and Technology Group and University of Tasmania, Primary supervisor* = **Author 1**
- *Dr Zhi Quan Leong, University of Tasmania, Co-supervisor* = **Author 2**
- *Dr Christopher Chin, University of Tasmania, Co-supervisor* = **Author 3**
- *Dr Alexander Forrest, University of California – Davis and University of Tasmania, Co-supervisor* = **Author 4**

Publication list and proportion of work details:

Paper 1 (Chapter 2), CFD modelling and validation of an Underwater Vehicle undergoing variable accelerations: *Candidate was the primary author and with author 1 and author 2 contributed to the conception and design of the research project and drafted significant parts of the paper. Authors 4 contributed to the interpretation of the work by critically revising the paper.* *Percentage of Contribution: Candidate: 77.5%, Author 1: 7.5%, Author 2: 12.5%, Author 4: 2.5%*
Paper 2 (Chapter 2), Simulation and validation of an Autonomous Underwater Vehicle in variable accelerations *Candidate was the primary author and with author 1 and author 2 contributed to the conception and design of the research project and drafted significant parts of the paper. Authors 4 contributed to the interpretation of the work by critically revising the paper.*

Percentage of Contribution: Candidate: 75%, Author 1: 7.5%, Author 2: 12.5%, Author 4: 5%
Paper 3 (Chapter 3), Numerical and experimental test of a marine propeller operating in a uniform fluid flow: *Candidate was the primary author and contributed to the planning, execution and preparation of the work for the research project and subsequent paper.* *Authors 2 contributed to the analysis and interpretation of the research data and the work by critically revising the paper.* *Percentage of Contribution: Candidate: 80%, Author 2: 20%*
Paper 4 (Chapter 4), Free running simulation of an Autonomous Underwater Vehicle undergoing a straight line manoeuvre via Computational Fluid Dynamics: *Candidate was the primary author and with author 1 and author 2 contributed to the conception and design of the research project and drafted significant parts of the paper.* *Authors 3 and 4 contributed to the interpretation of the work by critically revising the paper.* *Percentage of Contribution: Candidate: 72%, Author 1: 10%, Author 2: 12%, Author 3: 3%, Author 4: 3%*
Paper 5 (Chapter 5), Six-DOF simulations of an underwater vehicle undergoing straight line and steady turning manoeuvres: *Candidate was the primary author and with author 1 and author 2 contributed to the conception and design of the research project and drafted significant parts of the paper.* *Authors 3 contributed to the interpretation of the work by critically revising the paper.* *Percentage of Contribution: Candidate: 79%, Author 1: 10%, Author 2: 10%, Author 3: 1%*

We the undersigned agree with the above stated “proportion of work undertaken” for each of the above published (or submitted) peer-reviewed manuscripts contributing to this thesis

Signed:

……...	……...
Professor Dev Ranmuthugala	*Associate Professor Shuhong Chai*
Primary Supervisor	*Acting principal*
Australian Maritime College	*Australian Maritime College*
University of Tasmania	University of Tasmania
Date: 16/04/2018	Date: 18/04/2018

Acknowledgements

Thanks to Lord!

I am grateful to GOD for the good health and wellbeing that were essential to complete this thesis.

I wish to express sincere appreciation to Professor Dev Ranmuthugala and Dr Zhi Quan Leong for excellent guidance and leadership that enabled me to end up a PhD journey. I am indebted to them for sharing not only expertise and advice but also continuous encouragement throughout this project. Also, I would like to thank Dr Christopher chin and Dr Alex Forrest for the valuable comments and guidance. The supervisory team steered me in the right direction to complete this research.

I must express my very profound gratitude to my wife; Sookyung Lee for the patient love and unfailing support throughout the years of study. I would also like to thank to my parents (in law); Chunsik Kim, Youngim Yu, Manho Lee and Kyungim Yoo for their unceasing encouragement and support.

I am grateful to all church members of Launceston Full Gospel Church whose prayers were invaluable support.

I would take this opportunity to express gratitude to AMC staffs and my friends: Dr Jonathan Duffy, Dr Nagi Abdussamie, Dr Ahmed Swidan and Christopher Polis.

[Page intentionally left blank]

Abstract

This thesis presents the development of a validated six Degrees-of-Freedom (6-DOF) manoeuvring simulations of a fully appended BB2 generic submarine using Computational Fluid Dynamics (CFD). A build-up approach is used to first investigate the hydrodynamics of the vehicle's subcomponents individually, starting with the bare hull and propulsor models (i.e. a body force model and rotating model), progressing to the fully appended configuration for 6-DOF simulations that includes the hull, forward and aft control surfaces and a body force propeller.

The bare hull study involved prescribed motions (i.e. straight line, pure sway, and pure yaw) to examine the capability of the CFD model to predict the hydrodynamic forces and moments acting on the hull. The CFD predictions are validated, with good agreement, against experimental captive model measurements obtained at the Australian Maritime College Towing Tank (AMCTT). The propeller study involved hydrodynamic characterisation of a marine propeller operating in an open water condition. The global field quantities at various advance speeds are predicted using the CFD model, which were validated against experimental measurements provided by the Australian Maritime College Cavitation Research Laboratory (AMC CRL). Finally, the 6-DOF manoeuvring simulation study involves three generic manoeuvring tests (i.e. a straight line, steady turning and zig-zag manoeuvres) with a body force propeller and movable control planes commanded by an autopilot. The CFD predictions are validated against experimental free running measurements provided by Maritime Research Institute Netherlands (MARIN), showing that the 6-DOF manoeuvring CFD model is able to predict the vehicle`s trajectory and speeds with reasonable accuracy.

The developed CFD model and its methodology presented in this thesis can be used by underwater vehicle designers to carry out 6-DOF manoeuvring simulations for various vehicle designs, configurations and missions. The capability of 6-DOF manoeuvring simulations will enable the designers to determine a vehicle's manoeuvring characteristics for control system design and its safe operational limits.

[Page intentionally left blank]

Table of Contents

List of Figures

List of Tables

Nomenclature

A_D	Propeller disk area (m^2)
AOA	Angle of attack (degrees)
B	Breadth (m)
$C_{0.7R}$	Chord length at 0.7 propeller radius (m)
CB	Centre of buoyancy (m)
CG	Centre of gravity (m)
C_f	Frictional coefficient
d	Diameter (m)
D	Depth (m)
D	Diameter (m) [Chapter 3]
D	Fluid domain grid size (m) [Chapter 4]
D	Depth to deck (m) [Chapter 5]
D_{sail}	Depth to sail (m)
fb_x	Axial momentum source distribution
fb_θ	Theta momentum source distribution
F_T	Total force (N)
G	Centre of mass
H/D	Hub/diameter ratio
I	Moments and products of inertia for body
J	Advance coefficient
K, M, N	Moment vector obtained from integrated body surface pressure and shear
K_T	Thrust coefficient
K_Q	Torque coefficient
L	Overall length (m)
m	Mass (kg)
M_T	Total moment (Nm)
LCB	Longitudinal location of the centre of buoyancy (m)
LCG	Longitudinal location of the centre of gravity (m)
N	Yawing moment (Nm) [Chapter 2]
N'	Yawing moment coefficient (-) = $N/(0.5\rho U^2 L^3)$
p, q, r	Angular velocities (deg s^{-1})

$\dot{p}, \dot{q}, \dot{r}$	Angular accelerations (degrees s^{-2})
P	Pressure (Pa)
O	Inertial coordinate system
$\dot{r}$	Yaw acceleration (rad s^{-2}) [Chapter 2]
R_p	Radius of a propeller (m)
R_h	Radius of a propeller hub (m)
Re, Re_L	Length based Reynolds number (-) = UL/υ
Re_D	Diameter based Reynolds number (-) = UD/υ
S	Surface grid size
S_M	Sum of the body forces
T, t	Time (s)
u, v, w	Linear velocities (m s^{-1})
$\dot{u}, \dot{v}, \dot{w}$	Linear accelerations (m s^{-2})
U	Velocity of body centre of buoyancy relative to freestream velocity (m s^{-1})
U_0	Initial velocity in the x-axis (m s^{-1})
VCB	Vertical location of the centre of buoyancy (m)
VCG	Vertical location of the centre of gravity (m)
x, y, z	Body axis cartesian coordinates in the x,y,z-direction (m)
x_G	Longitudinal distance from the midship (m)
X	Longitudinal force (N) [Chapter 2]
X'	Longitudinal force coefficient (-) = $X/(0.5\rho U^2 L^2)$
X, Y, Z	Force vector obtained from integrated body surface pressure and shear
y_0	Amplitude (m)
∂y	First node wall distance (m)
Y	Lateral force (N) [Chapter 2]
Y'	Lateral force coefficient = $Y/(0.5\rho U^2 L^2)$
y^+	Non-dimensional wall distance (-) = $(u_* y_{wall})/\nu$
β	Drift angle (degrees)
ϕ, θ, ψ	Roll, pitch, yaw (degrees)
ρ	Fluid density (kg m^{-3})
τ	the molecular stress tensor
μ	Fluid dynamic viscosity (kg m^{-1} s^{-1})
μ_{eff}	Sum of dynamic viscosity and turbulence viscosity (kg m^{-1} s^{-1})

ω_t	Oscillatory frequency (s^{-1})
υ	Fluid kinematic viscosity ($m^2\ s^{-1}$) = μ/ρ
$\dot{v}$	Lateral acceleration ($m\ s^{-2}$)
δ	Total boundary layer thickness (m)
δ_r	Effective rudder angle (degrees)
δ_s	Effective sternplane angle (degrees)
η	Propeller efficiency
λ	Scale factor

Abbreviation

AMC	Australian Maritime College
AMC CRL	Australian Maritime College Cavitation Research Laboratory
AMCTT	Australian Maritime College Towing Tank
AUV	Autonomous Underwater Vehicle
AWT	Automatic Wall Treatment
BEMT	Blade Element Momentum Theory
BSLRSM	Baseline Reynolds Stress Model
CFD	Computation Fluid Dynamics
DARPA	Defense Advanced Research Projects Agency
DES	Detached Eddy Simulation
DNS	Direct Numerical Simulation
DOF	Degree-of-Freedom
DST	Defence Science and Technology
DTIC	Defense Technical Information Center
DTRC	David Taylor Research Center
EFD	Experimental Fluid Dynamics
FVM	Finite Volume Method
GGI	General Grid Interface
HPC	High Performance Computing
HPMM	Horizontal Planar Motion Mechanism
IFM	Inlet Flow Method
ISM	Immersed Solids Method
ITTC	International Towing Tank Conference
LES	Large Eddy Simulation
MARIN	Maritime Research Institute Netherlands
MDM	Moving Domain Method
MDT	Moving Domain Technique
MSS	Mesh Surface Size
Omega RSM	Omega-based Reynolds Stress Model
ONR	Office of Naval Research
OWT	Open Water Test

PMM	Planar Motion Mechanism
RANS	Reynolds Averaged Navier Stokes
RBD	Rigid Body Dynamics
RSM	Reynolds Stress Model
SASSST	Scale-Adaptive Simulation SST
SBD	System Based Design
SMB	Seakeeping and Manoeuvring Basin
SST	Shear Stress Transport
URANS	Unsteady Reynolds Average Navier Stokes
UUV	Unmanned Underwater Vehicle

Coordinate System

The submarine motion is described through a six Degree-of-Freedom (6-DOF) in body coordinate frame in which the origin (O) is located at the Centre of Gravity (CG) with the positive directions as shown below. The variables and notation of the frame are also defined below.

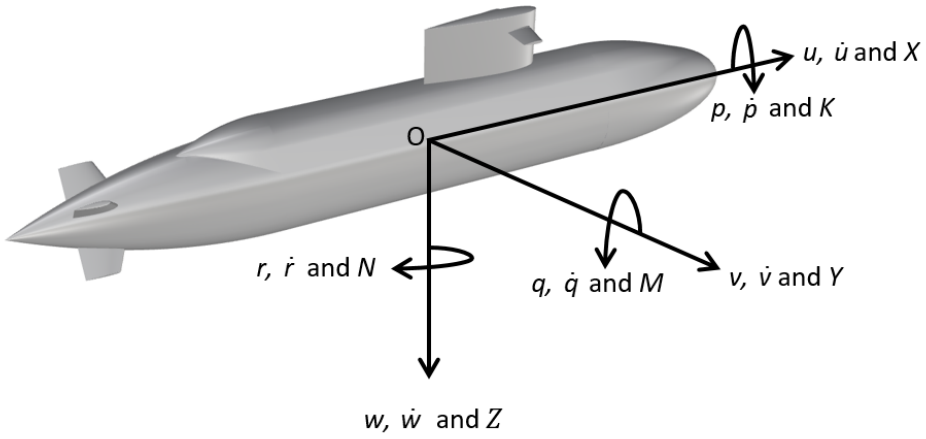

Body coordinate frame

Definition of the coordinate system and notations (ITTC, 2014)

DOF	Translation/ Rotation	Linear/ Angular Displacements	Force/ Moment	Linear/ Angular Velocities	Linear/ Angular Accelerations
1	surge	x [m]	X [N]	u [m s^{-1}]	$\dot{u}$ [m s^{-2}]
2	sway	y [m]	Y [N]	v [m s^{-1}]	$\dot{v}$ [m s^{-2}]
3	heave	z [m]	Z [N]	w [m s^{-1}]	$\dot{w}$ [m s^{-2}]
4	roll	ϕ [degrees]	K [Nm]	p [degrees s^{-1}]	$\dot{p}$ [degrees s^{-2}]
5	pitch	θ [degrees]	M [Nm]	q [degrees s^{-1}]	$\dot{q}$ [degrees s^{-2}]
6	yaw	ψ [degrees]	N [Nm]	r [degrees s^{-1}]	$\dot{r}$ [degrees s^{-2}]

[Page intentionally left blank]

Chapter 1: Thesis Introduction

1.1. Introduction

The motion control of underwater vehicles necessitates control systems that can adjust the control planes of the vehicle during a mission in order to maintain its trajectory and carry out required manoeuvres. As the control algorithms for the control planes are dependent on the vehicle's manoeuvring characteristics, it is essential to accurately determine the latter in order to design an adequate and accurate control system for the vehicle.

The manoeuvring characteristics of the vehicle can be examined using Computational Fluid Dynamics (CFD), experiment, or a combination of both through either coefficient-based or physics-based methods. The coefficient-based method implements standardised submarine motion equations (Gertler & Hagen, 1967; Abkowitz, 1969; Feldman, 1979; Fossen, 1994) comprising of a series of hydrodynamic coefficients determined by captive model tests (e.g. oblique tow, rotating arm and Planar Motion Mechanism (PMM) experimental programmes), numerical simulations (e.g. CFD) and/or analytical deductions. The coefficient-based method is commonly adopted as it is relatively fast and cost-effective for both CFD and experimental testings, but it is limited in accounting for the non-linear characteristics of the vehicle due to unsteady viscosity effects despite efforts to incorporate more complex non-linear models (Ross et al., 2007; Watt, 2007).

To address the limitation of the coefficient-based method and increase the accuracy in the determination of the manoeuvring characteristics, a physics-based method is implemented in this thesis. This method involves free running manoeuvres of the vehicle in response to its control planes, propulsor and the environment (see Figure 1-1). The free running test using CFD simulations involves the coupling of the governing fluid dynamics equations with Rigid Body Dynamics (RBD), enabling the prediction of the vehicle`s motion in the time domain.

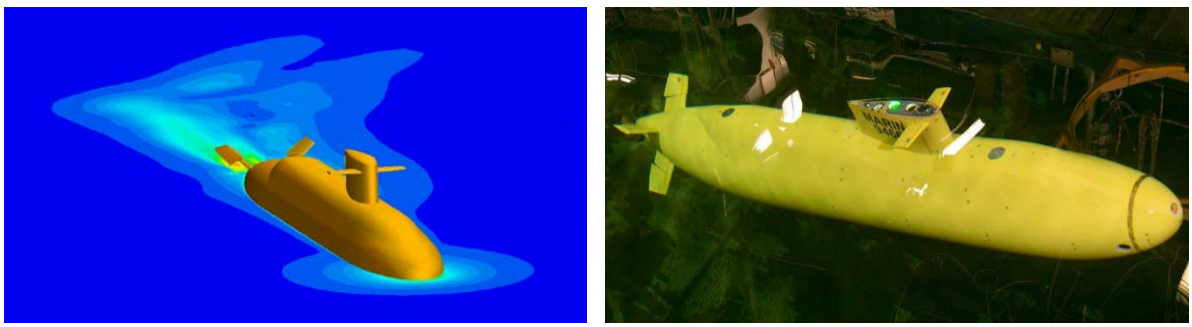

Figure 1-1: Free running models: (left) CFD simulation of a model scale submarine (Kim et al., 2018); (right) physical submarine model undergoing testing (Overpelt et al., 2015)

1.2. Problem Definition

In the past, experimental free running programmes have been the preferred option for physics-based determination of the manoeuvring characteristics (Itard, 1999; Issac et al., 2007; Jun et al., 2009; Overpelt et al., 2015). CFD free running simulations have rarely been conducted due to the complexity of the physical phenomenon involved with the vehicle`s hydrodynamics and the large computational resources required to perform simulations incorporating self-propulsion and moving appendages (Stern et al., 2013). These simulations involve fine computational grids and significantly small time step resolutions to capture the three dimensional transient flow characteristics around the physical shape of the appendages which continuously change position or deflect with time (ITTC, 2011a). Although this can be simplified with a body force model in which the influence of the appendages is resolved by applying additional body forces or momentum source (ITTC, 2011a), large computational resources are still required.

With increasing capabilities in both CFD and High Performance Computing (HPC), CFD free running simulation are becoming more affordable and are thus well suited to supplement experimental studies. However, the main difficulties and limitations of using CFD are that the accuracy of the results greatly depends on the experience of the analyst, the modelling such as grid refinement and the simulation settings such as turbulence modelling (ITTC, 2011a). Thus it is essential that the simulation models undergo verification through processes such as grid dependence studies and validation against experimental and full scale measurements.

1.3. Background

McDonald and Whitfield (1996), with a team of researchers at Mississippi State University and Pennsylvania State University, introduced a physics-based method for the trajectory prediction of self-propelled underwater vehicles (i.e. 6:1 prolate spheroid and the appended SUBOFF generic submarine geometry). The method used the three dimensional, time-dependent Reynolds Averaged Navier Stokes (RANS) equations coupled with the Six-Degrees of Freedom (6-DOF) vehicle motion equations (Gertler & Hagen, 1967) that were applied at each time step to solve the vehicle dynamics. The computations were carried out using their in-house

CFD code, UNCLE. The deflection of the control planes and the resulting effect on the vehicle were replaced by external control forces applied to the fixed control planes. The propeller was treated using two separate approaches: a body force model and an actual rotating propeller, although no direct comparison was made between the two approaches.

Zierke et al. (1997) continued the study of the physics-based method using UNCLE, focusing on the methodologies used in the physics-based simulation. Although this work significantly contributed towards the use of physics-based models to predict the manoeuvring characteristics of underwater vehicles, it was limited in terms of the time accurate motion of the vehicle appendages and the propeller rotating effect in the stern region. Zierke noted that future work needed to improve the computational efficiency and the coupling with the control algorithm to avoid accumulated path errors throughout a manoeuvre.

Pankajakshan et al. (2002) continued the analysis of the methodologies adopted in the physics-based simulation using UNCLE. The Unsteady Reynolds Averaged Navier Stokes (URANS) solver coupled with a 6-DOF rigid body model was used to simulate rudder-induced manoeuvres for rudder angles of up to 10 degrees. Deformable and regenerating gridding techniques were adopted for control surface movements and propeller rotation. Although the vehicle responded as physically expected, no validation was provided.

Phillips (2010) carried out a captive self-propulsion simulation with a body force propeller using the commercial CFD software, ANSYS-CFX. The propeller action was captured using a novel method of coupling a RANS solver with blade element momentum theory. However, the resulting propeller rotational speeds were substantially lower than those observed in the equivalent free running experiments. Phillips stated that the potential cause of the discrepancy was under-prediction of the vehicle drag, as the CFD analysis did not include the instruments and antennas protruding through the hull. Furthermore, development of the simulation was suggested for a free running manoeuvring simulation with time dependent action of the control planes.

Chase (2012) conducted CFD Open Water Tests (OWTs) of a rotating propeller, and attached it to a 1-DOF free running fully appended SUBOFF generic submarine hull, using the in-house CFD code, CFDShip-Iowa. The CFD results of the self-propulsion test were validated against

experimental measurements in terms of propulsion properties at one speed of 1.75 m/s. Although the CFD and experimental results showed good agreement, the work was limited in computing the vehicle`s straight line trajectory, speeds and accelerations due to DOF restrictions. Chase suggested further simulation coupled with a body force propeller model in lieu of a rotating propeller in order to increase the computational speed and thus reduce the simulation time.

Bettle (2013) investigated the development and testing of a 6-DOF submarine simulation capability that could be used to perform manoeuvring simulations using ANSYS-CFX. The simulation involved an URANS solver coupled with the solid body equations of motion (Gertler & Hagen, 1967) for the SUBOFF geometry, with applied body forces instead of a rotating propeller and deflecting control planes. Bettle recommended further studies on the following: modelling the rotating propeller and control plane deflections; autopilot in conjunction with dynamic deflection of the control planes; overset grid capability to avoid grid distortion or errors on complex geometries (e.g. fully appended submarine); comparison between 6-DOF URANS simulations with free running experimental measurements to validate the CFD model; and simulations using a more realistic submarine shape.

Coe (2013) performed CFD free running simulations of a General Purpose AUV (GPAUV). The CFD study involved URANS simulations coupled with a 6-DOF rigid body kinematic model using the commercial CFD software Star-CCM+. The deflection of the control plane was realised by an overset grid technique in conjunction with a body force propeller. Coe stated that conclusive evidence on the accuracy of the free running CFD model was not obtained from validation against experimental measurements, mainly due to issues in the experimental trials involving unexplained static offset of rudders (e.g. approximately 4 degree offset during the zig-zag manoeuvre). He also stated that the discrepancy between the CFD and experimental work may be attributed to the simulation model ignoring the D-rings fitted to the hull for deployment and recovery of the vehicle in the experiment. Coe suggested further work on: additional experimental measurements for further validation of the CFD simulations; performing a steady turning manoeuvre to provide additional insight into the sources of discrepancies between CFD and experimental results; and the improvement in the overset grid technique to reduce the excessive computational efforts due to very high grid refinement in gaps between the control planes and the adjacent ground board.

From this review of the literature, the notable limitations in CFD physics-based free running models were:

- the need to examine the capabilities of 6-DOF CFD free running simulations for underwater vehicles in conjunction with moving control planes commanded by an autopilot (McDonald and Whitfield, 1996; Zierke, 1997; Phillips, 2010; Bettle, 2013);

- the accurate application of a body-force propeller (i.e. actuator disk) instead of a rotating propeller to increase computational efficiency (Chase, 2012; Bettle, 2013); and,

- the comprehensive validation of free running simulations against experimental data for a number of manoeuvres to ensure the credibility of the CFD approach (Pankajakshan et al., 2002; Bettle, 2013; Coe, 2013).

1.4. Research Question, Objectives and Outcomes

The aim of this project is to investigate CFD capabilities as a System-Based Design (SBD) tool for 6-DOF free running manoeuvring simulations of a fully appended underwater vehicle. The motivation behind the study is that the developed 6-DOF manoeuvring simulations will enable the designers to determine a vehicle's manoeuvring characteristics for control system design and its safe operational limits. Thus, the main research question for this project is:

How can the 6-DOF manoeuvring simulations of a fully appended underwater vehicle be accurately performed using CFD, including the adequate representation of the propeller and control planes?

Due to the previously mentioned limitations and difficulties with CFD predictions, the approach is to:

- validate the CFD methodology against available experimental data for the hull and propeller of underwater vehicles; and

- apply the validated CFD methodology in free running simulations incorporating a 6-DOF underwater vehicle moving under the influence of the propeller and control planes.

This requires the project to address the following issues:

- What CFD methodology can be used to accurately predict underwater vehicle hydrodynamics?
- What modelling methods can be used to describe the motion of the vehicle moving freely in response to external forces?
- What propeller model (e.g. body-force and physically rotating models) and how can it be used to accurately and efficiently represent the propeller effect?
- What dynamic gridding techniques (i.e. sliding, re-gridding and overset) can be utilised to accurately and efficiently describe the dynamic control surface deflections?

Thus, the research focuses on delivering the following five main outcomes:

- An investigation into the accuracy of CFD predictions of hydrodynamic forces and moments acting on a deeply submerged underwater vehicle through quantitative validation against experimental measurements.
- Development of CFD methodology for free running simulation of underwater vehicles using an unappended vehicle moving in response to prescribed thrust forces.
- A study of CFD methodology for a rotating propeller model to provide an accurate prediction of the propeller performance characteristics for use in a body force propeller model.
- The 6-DOF CFD free running simulations of a fully appended hull with movable control planes and a body force propeller.
- Validation of CFD predictions for manoeuvring trials (i.e. straight line, steady turning and zig-zag manoeuvres) against experimental measurements.

1.5. Methodology

In order to achieve the outcomes, the project utilised a build-up approach to develop the 6-DOF manoeuvring simulation model using commercial CFD software and validation through experimental data. The build-up approach involves investigating the hydrodynamics of the vehicle's subcomponents individually, starting with the bare hull and propulsor models (including body force and rotating model options), and progressing to the fully appended 6-DOF simulation that includes the hull, forward and aft control surfaces and a body force propeller. The work is carried out through the following phases:

Phase 1: Develop a verified and validated CFD model to predict the hydrodynamic coefficients of the underwater vehicle without a propulsor.

Phase 2: Characterise the propeller performance properties (i.e. K_T, K_Q and η) of the vehicle's propeller through verified and validated CFD simulations.

Phase 3: Develop a CFD manoeuvring simulation model of the vehicle under a prescribed thrust force and a body force propeller model respectively in 1-DOF and an even keel condition.

Phase 4: Develop a 6-DOF CFD manoeuvring simulation model of the vehicle operating with movable control planes and a body force propeller that incorporates the prescribed propeller performance characteristics obtained from captive self-propulsion simulations using a rotating propeller.

Phase 5: Validate the 6-DOF CFD simulation model against experimental measurements.

1.6. Limitations of the present studies

The main limitations of the present studies are as outlined below:

- The body force propeller used in the free running simulations is an actuator disk in which prescribed momentum sources, based on thrust and torque were obtained from a CFD captive self-propulsion test under uniform fluid flow. This limits an accurate representation of the fluid flow field when operating in non-uniform conditions.

Although the limitation influenced diminutive on the manoeuvring characteristics in the manoeuvring trials (i.e. straight line, steady turning and zig-zag manoeuvres) presented in this thesis, it could be significant for extreme manoeuvres (e.g. emergency rising or collision avoidance), involving a non-uniform axial velocity field that leads to tangential and radial variations in the propeller thrust and torque.

- The current study used model scale vehicles for all simulations. The results are limited in application to a full-scale vehicle due to the possible scale effects caused by different boundary layer profiles and flow separation on the vehicle.

1.7. Novel Aspects and Significance of the Study

The present research makes an original contribution to the use of CFD as a tool to predict the hydrodynamic characteristics and manoeuvring performance of an underwater vehicle. There are three significant contributions as outlined below.

- There is very little research in the public domain on 6-DOF free running simulations of an underwater vehicle with moving control planes and a propeller. This is mainly due to the difficulty of simulation modelling and the requirement of significant computational resources. The present study developed a 6-DOF free running simulation model incorporating dynamic deflection of the control planes using an overset grid technique and a body force propeller model to reduce computational requirements.

- This thesis provided the validated CFD methodologies for the individual component (i.e. hull and propeller) of an underwater vehicle, and its application to a free running simulation model. The model proved the validity of the methodologies through using different hull forms and propeller geometries. The proposed methodologies will contribute to the knowledge in the development of free running CFD simulations.

- To date, validation of CFD free running simulations of an underwater vehicle in 6-DOF have not been extensively reported in the public domain. With the availability of published experimental data (Overpelt et al., 2015), the developed CFD manoeuvring model is validated for the straight line, steady turning and zig-zag manoeuvres.

1.8. Vehicle and Propeller Geometries

The geometries of the vehicles and propellers used for the work in Section 1.5 are as follows:

Phase 1 used a scaled axisymmetric SUBOFF submarine hull form shown in Figure 1-2 (Groves et al., 1989) developed by the Defence Advanced Research Projects Agency (DARPA). The un-appended SUBOFF hull from has a length of 1.440m and a diameter of 0.181m respectively.

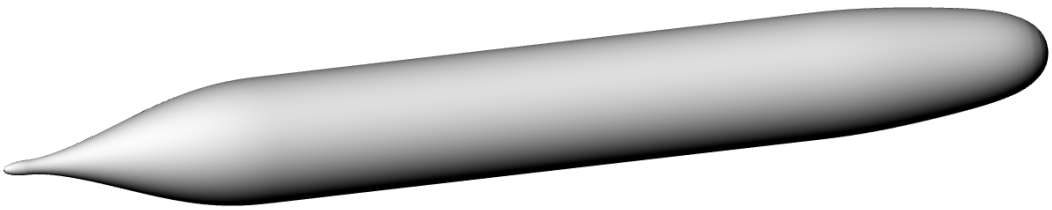

Figure 1-2: Axisymmetric un-appended SUBOFF submarine hull form (Groves et al., 1989) developed by the Defence Advanced Research Projects Agency (DARPA)

Phase 2 used a 5-blade propeller DSTO 115-1 shown in Figure 1-3 designed by the Defence Science and Technology (DST) group (Norrison et al., 2016). The propeller has a diamter of 0.25m with a hub-to-diameter ratio of 0.2:1 and a pitch of 0.3m at 70% of the propeller radius.

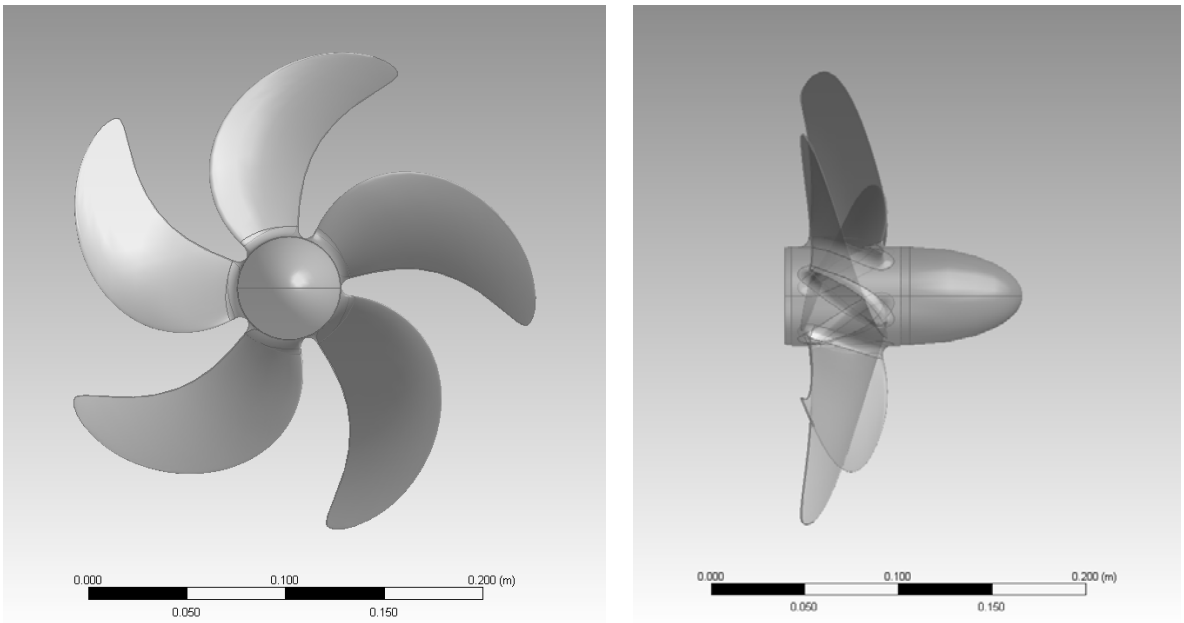

Figure 1-3: DST five blade propeller, DSTO 115-1, (Norrison et al., 2016)

Phase 3 used two bare hulls (i.e. a 6:1 length-to-diameter ratio prolate spheroid with a length of 1.5m and the un-appended SUBOFF hull same as that in Phase 1), and a fully appended SUBOFF generic submarine model shown in Figure 1-4 (Groves et al., 1989), with a length of 4.36m and a diameter of 0.51m.

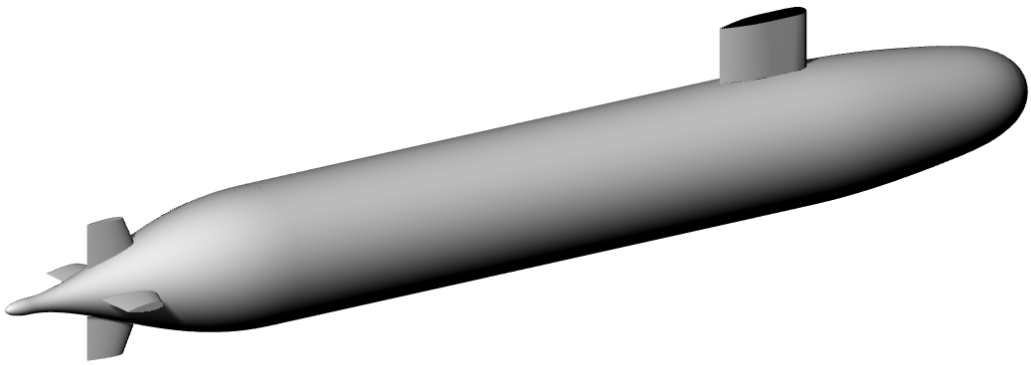

Figure 1-4: Appended DARPA SUBOFF generic submarine geometry (Groves et al., 1989)

Phase 4 and 5 used a scaled generic DST/MARIN BB2 generic submarine geometry (Overpelt et al., 2015) shown in Figure 1-5, which represents a typical SSK- submarine. This design was derived from the hull form introduced by Joubert (2006). The BB2 geometry has a length of 3.826m and a breadth of 0.523m.

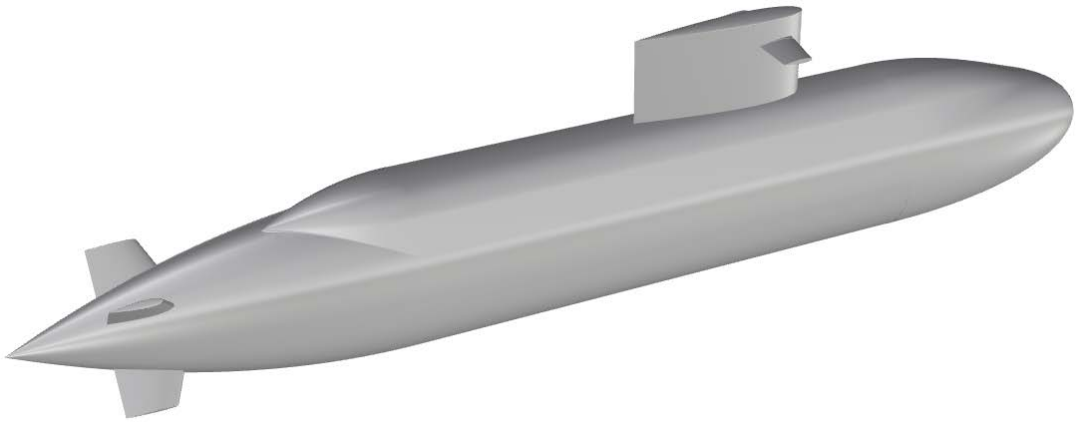

Figure 1-5: DST/MARIN BB2 generic submarine geometry representation a typical SSK-submarine. The design was derived from hull form introduced by Joubert (2006)

1.9. Thesis Structure

The thesis follows a "chapterised" structure, which is composed of: an introduction in Chapter 1; a collection of peer reviewed published or submitted scientific papers in Chapters 2 to 5, including additional information as required; the conclusions on the research findings in Chapter 6; and Appendices. Note that the simulations conducted in Chapters 2 to 4 were performed using ANSYS-CFX v14.5, while those in Chapter 5 were based on Star CCM+ v11.02. This was owing to limitations in ANSYS-CFX, especially the absence of a built-in capability of defining a local coordinate for moving appendages and overset grid capability. A summary of Chapters 2 to 6 and the Appendices is provided below.

Chapter 2: Examines the numerical and experimental methodology in the prediction of the hydrodynamic coefficients of an underwater vehicle undergoing prescribed manoeuvres. A Horizontal Planar Motion Mechanism (HPMM) test is performed using the un-appended SUBOFF (see Figure 1-2) undergoing straight line, pure sway and pure yaw manoeuvrers. This study is to ensure the accuracy of the hydrodynamic predictions using the appropriate CFD methodology, which forms the basis for the free running simulations.

Chapter 3: Examines CFD methodology for the predictions of the open water propeller performance characteristics (i.e. K_T, K_Q and η) using the 5-blade DSTO 115-1 propeller (see Figure 1-3). The predictions are validated against open water experimental measurements of the model scale propeller (Norrison et al., 2016) in the Australian Maritime College Cavitation Research Laboratory (AMC CRL). The developed CFD methodology is adopted in the captive self-propulsion simulations to provide the propeller performance characteristics for a body force propeller model utilised in in the free running simulation. A brief introduction of the body force propeller model is also presented.

Chapter 4: Investigates the CFD capability of free running simulation models using unappended hull forms i.e. the 6:1 prolate spheroid hull and the un-appended SUBOFF hull form (see Figure 1-3) and the appended SUBOFF (see Figure 1-4) in 1-DOF under an even keel condition. This study includes two propulsion modelling options: a prescribed thrust force and a body force propeller model (i.e. actuator disk). These studies provide a foundation for

the 6-DOF CFD free running model to accurately simulate the motion of the vehicle in response to the selected propulsion model.

Chapter 5: Presents the 6-DOF free running manoeuvring simulation model of a scaled BB2 submarine (see Figure 1-5) consisting of moving control surfaces and a body force propeller model using an actuator disk. The study involves two manoeuvring trials (i.e. straight line and steady turning manoeuvres) in 6-DOF with validation against experimental measurements of the vehicle conducted at MARIN (Overpelt et al., 2015). In addition, initial results and validation work for a zig-zag manoeuvre is also presented. The latter work will be completed and published in near future.

Chapter 6: The concluding chapter provides a brief summary of the project followed by the body of the chapter that collates the findings and outcomes from the various chapters. These conclusions are then discussed in terms of the implications of the research and possible future work to address issues raised within the project, and to allow further development of free running model simulations.

Appendix I: Provides information on setup of the dynamic grid techniques to model the dynamic motion of a hull.

Appendix II: Outlines the uncertainty analysis of the experimental data for Chapter 2.

[Page intentionally left blank]

Chapter 2: Simulation of Captive Model

This chapter has been published in the International Society of Offshore and Polar Engineering (ISOPE) conference and International Journal of Offshore and Polar Engineering (IJOPE). The citation for the research article is:

Kim, H., Leong, Z.Q., Ranmuthugala, D., & Forrest, A. 2014, 'CFD modelling and validation of an Underwater Vehicle undergoing variable accelerations', *International Society of Offshore and Polar Engineering (ISOPE) conference*

Kim, H., Leong, Z.Q., Ranmuthugala, D., & Forrest, A. 2015, 'Simulation and validation of an Autonomous Underwater Vehicle in variable accelerations', *International Journal of Offshore and Polar Engineering (IJOPE).*

This chapter has been removed for copyright or proprietary reasons.

[Page intentionally left blank]

Chapter 3: Propeller Modelling

This chapter consists of two sub-chapters:

Part 3A- Rotating Propeller

Part 3B- Body Force Propeller

[Page intentionally left blank]

PART 3A: Rotating Propeller

This sub-chapter has been submitted for review to the Journal of Ships and Offshore Structures.

Abstract

This paper presents an investigation of the hydrodynamic characteristics of a five-bladed marine propeller operating in a uniform flow field through numerical and experimental tests. The global field quantities, thrust (K_T) and torque (K_Q) coefficients, as a function of the advance coefficient (J) were predicted through Computational Fluid Dynamics (CFD) simulation using Reynolds Averaged Navier-Stokes (RANS) equations. Validation of the CFD simulation was carried out using the experimental measurements conducted at the Australian Maritime College Cavitation Tunnel (AMCCT). The major challenge for the RANS simulations is that the results greatly vary with the numerical model settings. Thus, the present study discusses the simulation settings including selection of the turbulence model in association with near wall gridding and other factors such as state condition and time discretisation to achieve predictions comparable to experimental measurements. The CFD predictions were found to be in good agreement with the experimental measurement (i.e. less than 5% at up to J =1.1 and 10% at up to J =1.19 for K_T and K_Q). The comparison of the numerical predictions with the experimental measurements reveals that the appropriate selection of the turbulence model, boundary conditions, and the quality of the grid is critical to predictions of high fidelity for a propeller.

3.1. Introduction

The investigation of the hydrodynamic performance of a propeller is imperative for a marine vehicle operating efficiently at a desired speed. Ideally, an efficient propeller should provide maximum thrust and minimum torque for the optimum propeller rotation speed. These characteristics can be assessed via propeller hydrodynamic performance curves representing thrust coefficient, torque coefficient, and efficiency as a function of advance speed ratio. These propeller performance indicators (also known as global field quantities) are obtained through an Open Water Test (OWT) that involves a propeller operating in a uniform fluid flow.

The OWT can be performed via numerical simulation using Computational Fluid Dynamics (CFD) or Experimental Fluid Dynamics (EFD). With the ongoing development of CFD technology and computer performances, CFD is increasingly used in the hydrodynamic analysis of propellers (Joung et al. (2010); Lu et al. (2012); Guilmineau et al. (2014); and Song et al. (2015)). However, the accuracy and reliability of a CFD simulation are still susceptible to the simulation settings, including grid strategy and physics model used. Morgut and Nobile (2012) studied the influence of grid type (i.e. hybrid-unstructured and hexa-structured grids) and turbulence model using Baseline Reynolds Stress Model (BSLRSM) and Shear Stress Transport (SST) for the RANS computation of a propeller characteristics in open water condition. The study indicated that the both grid types can provide similar levels of accuracy of the global field quantities unless detailed investigations of the flow field are needed, and the BSLRSM provided only slightly better predictions than the SST. However, the influence of near wall gridding and time discretisation on the predictions were not explored.

The present study examines the thrust, torque and efficiency characteristics of a 5-blade propeller operating in a uniform flow field at various advance velocities, through CFD prediction with EFD validation. The study also examines the influence of various CFD simulation settings that can affect the predictions. Five different omega-based turbulence models with various near wall grids strategies involving first node y^+ and inflation layer thickness were evaluated. Other factors that influence the prediction such as time discretisation and state conditions (i.e. steady-state and transient) are also investigated. The CFD predictions were validated against EFD measurements conducted at the AMC cavitation tunnel. From this

study, the authors anticipate the developed methodology to be used for propeller modelling in a free-running CFD simulation for marine vessels.

3.2. Methodology

3.2.1. Propeller Model

The present study utilised a 5-blade propeller designed by the Defence Science and Technology (DST) group (Norrison et al., 2016) (see Figure 3-1). The propeller principal dimensions are outlined in Table 3-1.

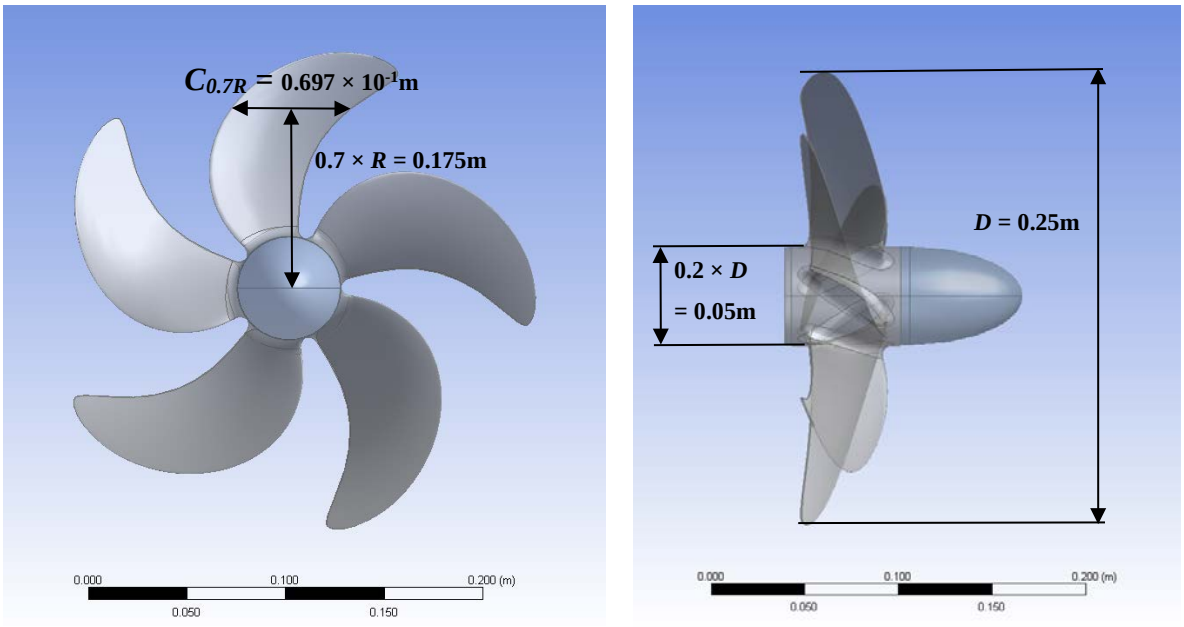

Figure 3-1: DST 5-blade propeller

Table 3-1: Specification of the DST 5-blade propeller

Description	Symbol	Values	Unit
Number of blades		5	-
Hub diameter ratio	H/D	0.20	-
Diameter	D	0.25	m
Propeller disk area	A_D	49.087 × 10^{-3}	m^2
Chord at 0.7 radius	$C_{0.7R}$	0.697 × 10^{-1}	m

3.2.2. Numerical Programme

a. Simulation setup

The numerical OWTs were conducted using RANS equations with the commercial CFD software, ANSYS CFX v16. Double Precision mode was adopted throughout the simulations to minimise rounding-off errors.

The numerical tank size was prescribed the same as the size of the experimental tank. The boundary conditions applied are: no-slip walls on the propeller and mounting strut; inlet condition with a specified flow velocity; and an opening boundary with zero relative pressure at the top, side and bottom boundaries (see Figure 3-2). The single-phase fluid was prescribed as fresh water, incompressible, and isothermic. The general simulation settings used include employed the high-order advection scheme.

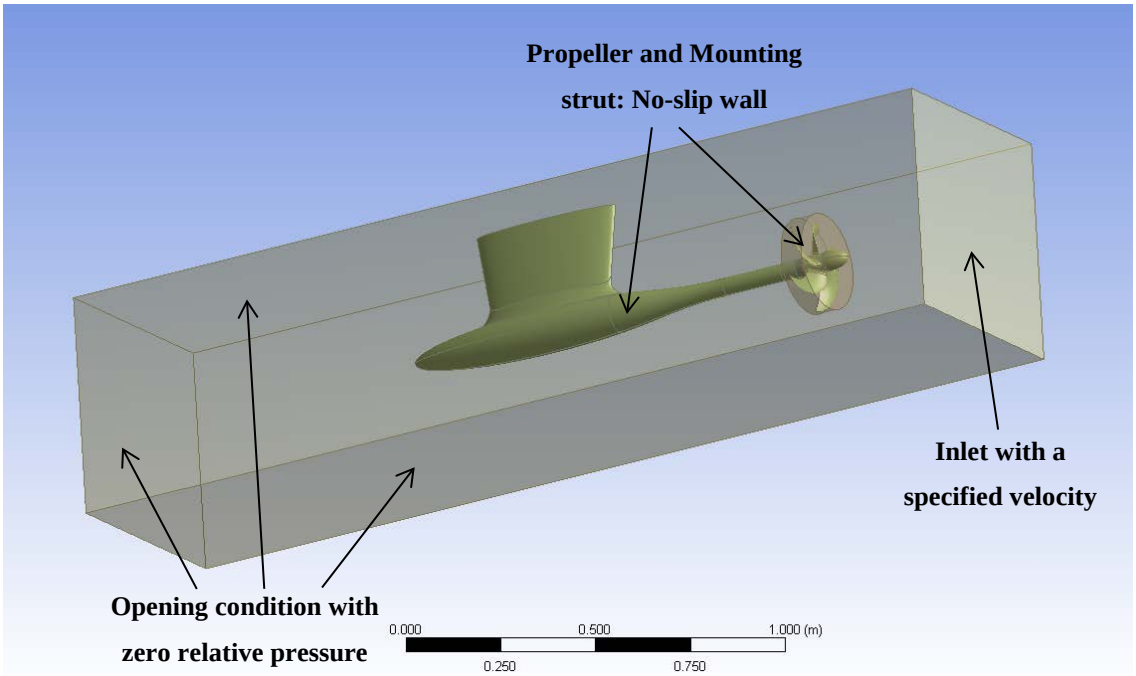

Figure 3-2: Boundary conditions and arrangement of the propeller in the numerical tank

b. Grid dependence study

The element size of the grid play an important role in the computation as these influence the convergence of values and the computation time. Due to the complexity of the propeller geometry, an unstructured tet-grid was selected for its ability to represent the complex geometry without excessive time demand. Inflation layers consisting of tet-prisms were applied on surface of the propeller and mounting strut to capture the boundary layer. The investigation kept a y^+ of 12.5 which is the smallest value used for its influence (see section 2.3). Note that the y^+ is defined as the dimensionless distance measured from the wall surface to the edge of the first layer. The first node wall distance (∂y) reflected by the y^+ value as shown in equation (3-1).

$$\partial y = L \times \partial y^+ \sqrt{80}\,\mathrm{Re}^{\left(-13/14\right)} \tag{3-1}$$

In order to establish the grid requirements for the propeller simulation, a grid dependence study was carried out to ensure the simulation results were consistent and independent of the grid density. Figure 3-3 shows the percentage difference of K_T and K_Q for each grid level compared to those for the finest grid level (i.e. 14.5 million). The propeller rotation speed was set at 15 rps at 4.46m/s of a uniform fluid speed, which is the maximum speed set in the experiment. The results show that further grid refinement beyond a 9 million grid affects the K_T by less than 0.6% and the K_Q by less than 0.4%. However, the required computation time was significantly increased by around 4 times. Given the computational efficiency as well as the acceptable accuracy, the present study adopted a 9 million grid with an associated 0.6% uncertainty in the predicted values.

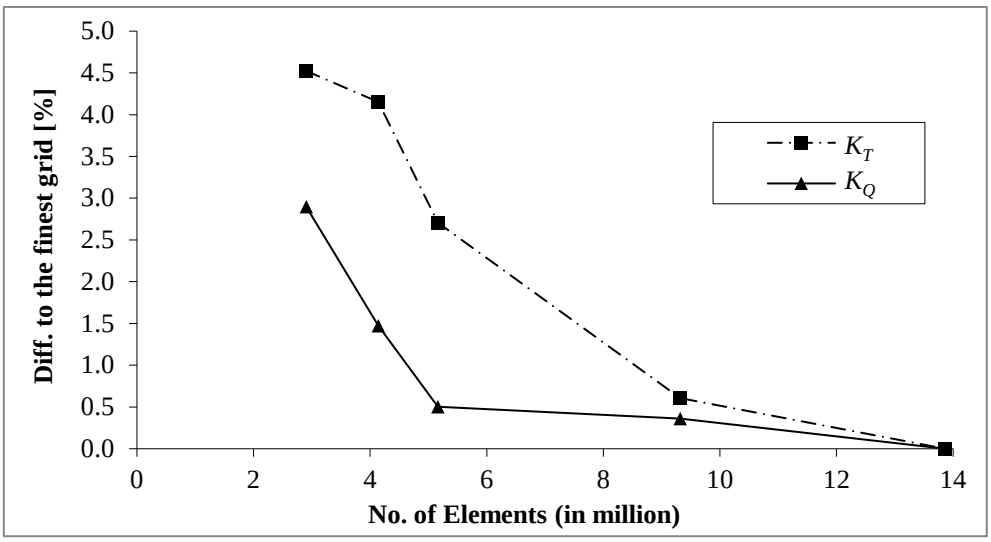

Figure 3-3: Grid dependence study at 15rps and 4.46m/s inlet flow velocity

c. Near wall gridding with RANS omega-based turbulence model selection

The evaluation of the near wall gridding treatment with different RANS turbulence model was carried out using omega based RANS models. The turbulence models include the Baseline Reynolds Stress Model (BSLRSM), standard k-omega (k-ω), Shear Stress Transport (SST), omega-based Reynolds Stress Model (Omega RSM), and the Scale-Adaptive Simulation SST (SASSST). The near wall gridding treatment was examined as function of the first inflation layer height (reflected by y^+).

In ANSYS CFX, the omega based RANS models utilise the Automatic Wall Treatment (AWT) model for boundary layer modelling. The AWT dictates if the simulation uses the low-Reynolds wall treatment or the wall function formulation for the boundary layer depending on the first layer y^+ (ANSYS, 2012). The current study focuses on using the wall function to reduce computational cost and allow higher mesh resolution efforts on the surface of the blades. The AWT in ANSYS CFX effectively switches to the wall function formulation at y^+ values of 11.06 and above (Hally, 2009). It is also important that the first layer y^+ does not exceed the log-law region of the boundary layer Thus, the simulations in this study were performed with y^+ values ranging from 12.5 to 120.

Figure 3-4 shows the K_T and Kq predictions of the different turbulence models at various y^+ values and the EFD measurements with an error bar indicating the experimental errors (i.e. K_T = 4.2% and K_Q = 10.2%). The simulations were conducted with the maximum inlet speed from the experiment, i.e. 4.46 m/s, and a propeller rotation speed of 15 rps.

At y^+ =12.5, the K_T was under-predicted compared to the experimental measurements. This is like due to the first layer height being too far into the buffer region of the boundary layer for the wall function to be valid. At y^+ = 25, the first wall-adjacent node deemed placing in the log law layer, resulting in the minimum descripancy of K_T and K_Q over the various turbulence models. However, at y^+ = 50, 75 and 120, the errors of K_T and K_Q become larger due to insufficient resolution in the log law layer. This shows that the lower y^+ enables the better resolution in the log layer region, thus providing the better predictions in K_T and K_Q.

Overall, although SST, SASSST and K-omega provided stable prediction of K_T and K_Q than Reynolds stress models (i.e. Omega-RSM and BSLRSM) throughout the y^+ ranges, the Reynolds stress models perform better at lower y^+ values (e.g. 12.5 and 25) where the better resolution of log layer was achieved. Further, the BSLRSM with y^+ = 25 provided the most accurate predictions in comparison with the EFD measurements (provided by the current EFD testing), thus the combination of BSLRSM and y^+ = 25 was adopted for the remainder of this study.

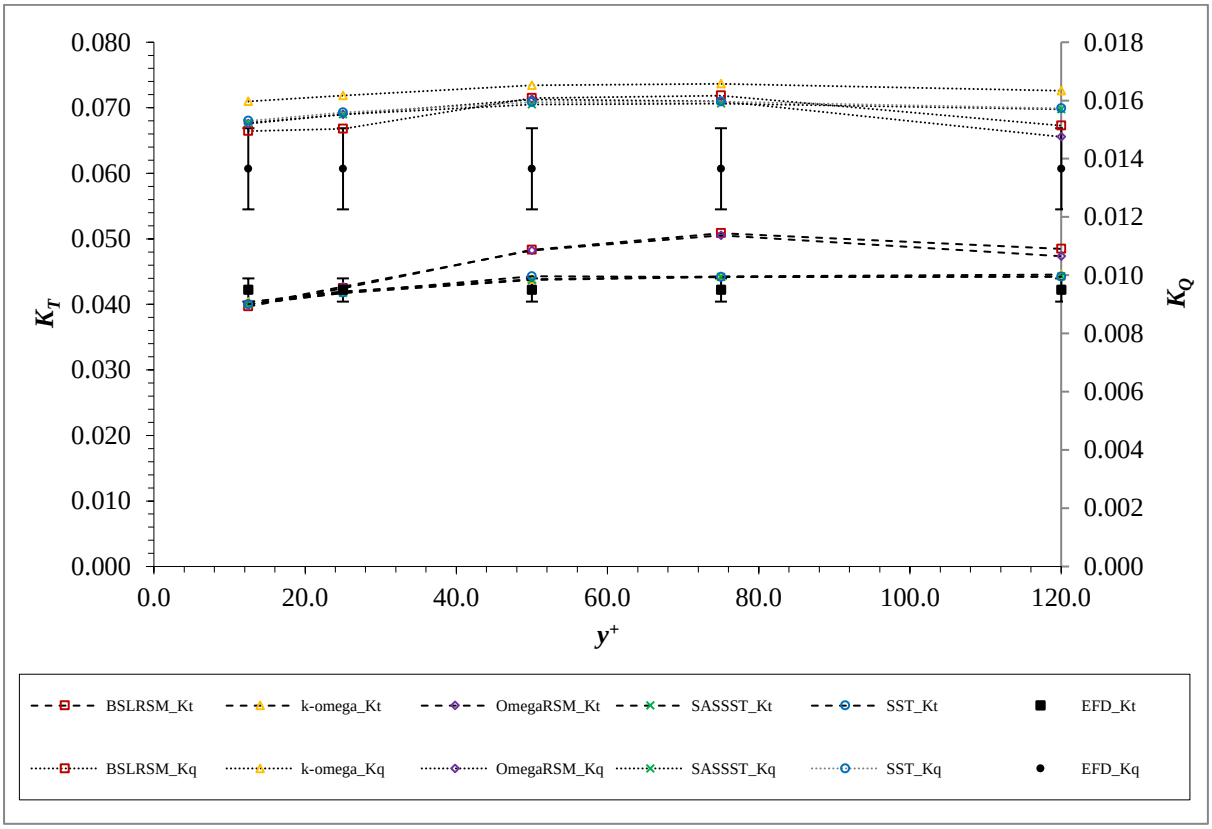

Figure 3-4: Comparison of the K_T and K_Q between EFD data and CFD prediction using a number of turbulence models at various y^+ values (at 15 rps and 4.46 m/s inlet flow velocity), and the EFD measurements with an error bar indicating the experimental errors (i.e. K_T = 4.2% and K_Q = 10.2%)

d. Boundary layer thickness

Various total inflation layer thicknesses were applied to ensure that the boundary layer is sufficiently enclosed within the prescribed inflation layers. A number of thicknesses were

estimated based on the experimental based typical boundary layer thickness (i.e. $20 \times 10^{-3} \times C_{0.7R}$) by Carlton (2012), and theoretical estimation by Prandtl (1935) for turbulent flow on a plate, $(0.16 \times C_{0.7R}) / \mathrm{Re}_{C_{0.7R}}^{1/7}$, where $C_{0.7R}$ (i.e. 0.697×10^{-1}) is the maximum span length of the propeller at 0.7 times radius from the centre (White, 2011). As Prandtl`s estimation is for a flat plate, seven different thicknesses (see Table 3-2) were examined to investigate the sufficient thickness to capture the boundary layer around the curved geometry of the propeller. The investigation was conducted using the BSLRSM turbulence model and a y^+ value of 25.

Table 3-2: K_T and K_Q predictions adopting various total inflation layer thicknesses (at 15 rps and 4.46m/s inlet velocity)

Property	Value	Unit
Carlton (2012)	1.40×10^{-3}	m
0.25 × Prandtl's estimate	4.411×10^{-4}	m
0.50 × Prandtl's estimate	8.821×10^{-4}	m
1 × Prandtl's estimate	1.764×10^{-3}	m
2 × Prandtl's estimate	3.529×10^{-3}	m
3 × Prandtl's estimate	5.293×10^{-3}	m
4 × Prandtl's estimate	7.057×10^{-3}	m
5 × Prandtl's estimate	8.821×10^{-3}	m

Figure 3-5 shows the prediction of the K_T and K_Q as a function of the total inflation layer thicknesses on the blade surface. Both the predicted K_T and K_Q values were found to be independent of the total inflation layer thickness when the thickness value was 5.297×10^{-3} m (3 × Prandtl's estimate) and above. The predictions from values smaller than this thickness (i.e. Carlton, and 0.25 , 0.5, 1 and 2 of Prandtl's estimate) was found to decrease and is attributed to the boundary layer exceed the total inflation layer thickness (Carlton, 2012). As a conservative measure, a total thickness of the inflation layers corresponding to three times Prandtl's estimate was used for the remainder of the study.

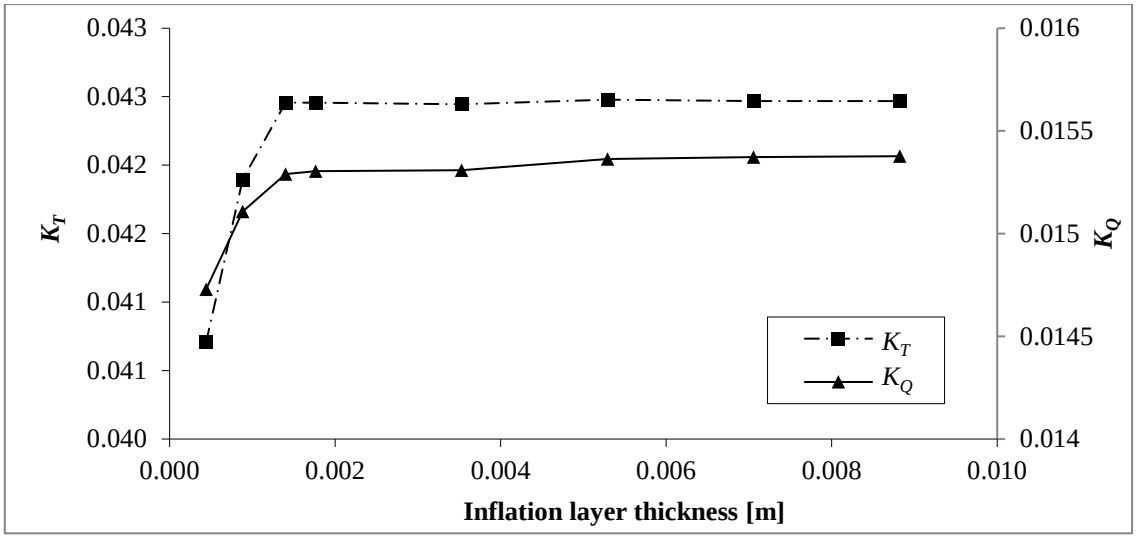

Figure 3-5: K_T and K_Q predictions over a number of total inflation layer thicknesses

e. Time discretisation

ANSYS CFX is an implicit solver which does not require a Courant number to be maintained below 1 for numerical stability (ANSYS, 2012). Nonetheless, a series of simulations utilising different time steps were conducted to establish the optimal time step whereby its effect on the predictions are negligible. The maximum normalised residuals for mass and momentum were maintained below 1×10^{-4} using a maximum of six inner iteration loops per time step.

Table 3-3 shows the percentage difference in K_T and K_Q for four time steps compared to the predictions of the smallest time step (5×10^{-4} s) used in this study. The results show that a maximum difference of up to 0.14% over the time step values investigated. Thus, the time step of 0.005s was used in the rest of the simulations presented in this study.

Table 3-3: Percentage difference of the K_T and K_Q against the smallest time step (i.e. 5×10^{-4}s)

Time step [s]	K_T	K_Q
1×10^{-2}	0.134	0.089
5×10^{-3}	0.107	0.089
1×10^{-3}	0.107	0.089
2.5×10^{-4}	0.080	0.060
5×10^{-4}	–	–

f. Steady-state vs Transient simulations

The influence of two different state conditions (i.e. steady-state and transient) on the predictions were examined. The steady-state simulation adopted a frozen rotor method. This utilises a rotating reference frame with the predictions based on the change of reference frame with respect to the relative fixed orientation of the propeller over the interface. On the other hand, the transient simulation uses a rotor stator method that predicts the true transient interaction of the flow by simulating the transient relative motion between the components on each side of the General Grid Interface (GGI) connection. The frozen rotor method reduces the computational loads compared to the transient rotor stator as it allows a steady-state representation of the flow around the propeller. Table 3-4 shows the percentage difference of K_T and K_Q predictions between the steady-state and transient simulations. The maximum difference was up to around 3%. As this difference is deemed acceptable in terms of the effect of the state condition, the remainder of the study in this paper used the steady state simulations due to savings in the computational resource.

Table 3-4: Percentage difference of the K_T and K_Q in the transient condition compared to that in the steady-state for the propeller operating at various inlet flow speeds at 15 rps

Inlet speed [m/s]	K_T	K_Q
1.974	-1.38	2.47
2.446	-1.95	2.86
3.067	-1.85	2.87
3.685	-0.93	2.44
4	0.20	2.32

3.2.3. Experimental Setup

An experimental test was performed at the AMCCT (see Figure 3-6) using the 5-blade propeller. This test involved the measurement of the propeller thrust and torque characteristics while operating in a uniform flow field. Measurements of mean thrust and torque were made for a range of tunnel velocities at a fixed rate of revolution of 15 rps. It is noted that the blockage correction was made in the experimental data to avoid the interference due to the confinement

of the test section walls. This enables the experimental data comparable with those that would be obtained in an infinite flow field.

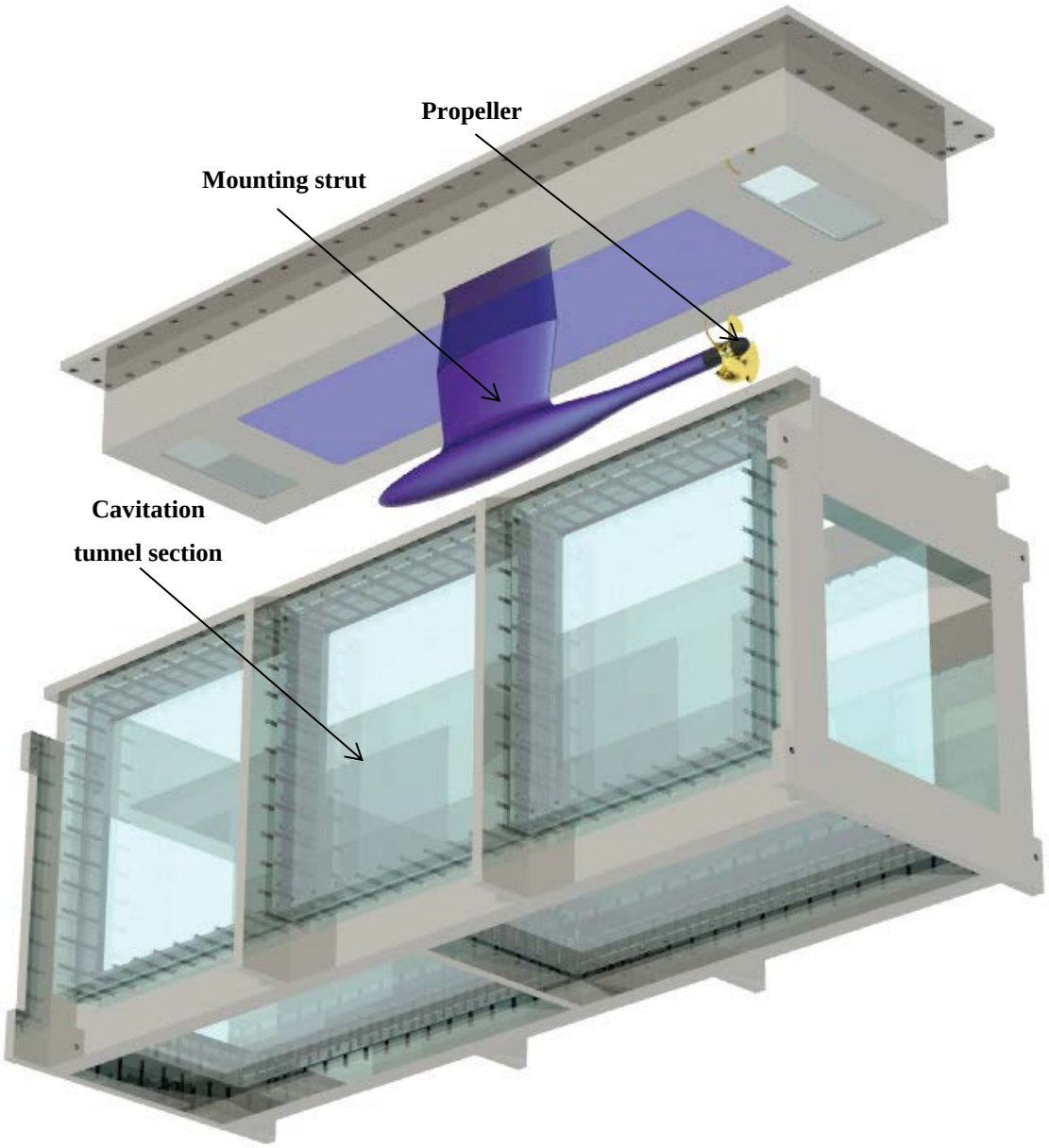

Figure 3-6: Arrangement of the propeller dynamometer and cavitation tunnel section

3.3. CFD predictions vs EFD measurements

The open water test was conducted at various advance speeds at a fixed rotational speed (i.e. 15rps or 900rpm). The inlet speeds varied from 1.97m/s to 4.47m/s. Figure 3-7 shows K_T, K_Q and efficiency (η) as a function of advance coefficient ratio. The CFD predictions are found to

be a good agreement with EFD measurement (Norrison et al., 2016) with a maximum discrepancy of up to 3.5% for K_T at J =1.97 and up to 10.2% for K_Q at J = 1.19. The discrepancies were found to reduce as the advance coefficient decreases. Up to J=1.021, both CFD and EFD data showed a very good agreement with a less than 4% difference for both K_T and K_Q. This is attributed to the sensitivity limit of the measurement in EFD whereby the values of the thrust and torque become increasingly difficult to measure as they decrease as the advance coefficient increases.

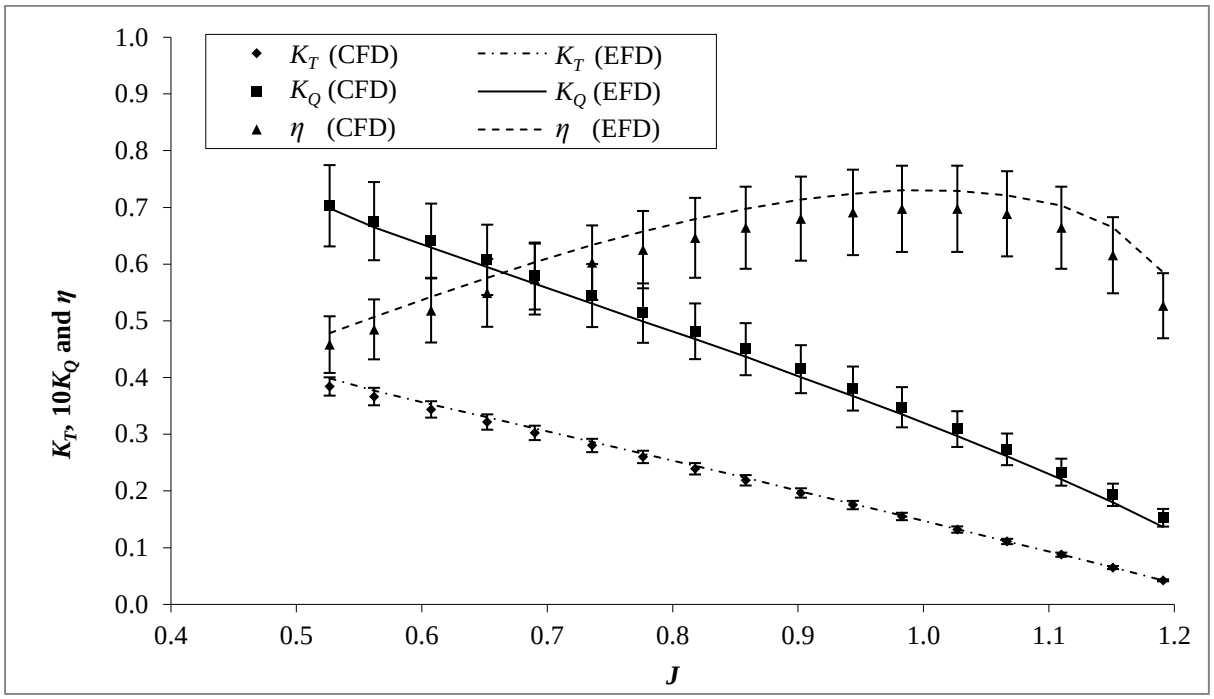

Figure 3-7: Comparison of the K_T, K_Q and efficiency (η) between CFD predictions and EFD measurements (Norrison et al., 2016) over the advance coefficient (J) from 0.527 to 1.191, error bars indicate the maximum experimental errors (i.e. K_T = 4.2%, K_Q =10.2% and η = 10.9%)

3.4. Conclusions and recommendations

This paper presented the numerical and experimental investigations of a propeller operating in a uniform fluid flow in order to examine the performance characteristics of a five bladed propeller was investigated numerical using CFD. The CFD model was validated via experimental measurements. The numerical study included detailed methodology of RANS-based simulation containing the turbulence model selection among the omega-based turbulence

models with the required grid conditions (i.e. first mesh layer height, y^+ and total inflation layer thickness), also including the appropriate simulation settings (i.e. steady-state and transient conditions, and time step). In order to reduce computational load associated with the grid resolution, the wall formulation was used in modelling boundary layer for the simulations.

Five omega based turbulence models were investigated in this study: the Baseline Reynolds Stress Model (BSLRSM), standard k-omega (k-ω), the Shear Stress Transport (SST), the Omega-based Reynolds Stress Model (Omega RSM) and the Scale-Adaptive Simulation SST (SASSST). It was found that the BSLRSM predictions at $y^+ = 25$ provided the most promising results with good agreement against the experimental measurements.

Investigation of the effect of total inflation layer thickness on the numerical predictions recommends that the minimum thickness to be at least be equal to Prandtl's $1/7^{th}$ power law estimate of a turbulent boundary layer thickness over the maximum span length of the propeller at 0.7 times radius from the centre. Under-prescribing the total thickness resulted in lower K_T and K_Q predictions compared to the recommended thickness, while over-prescribing the total thickness showed no perceptible differences in prediction.

Overall results showed that, in comparison to the EFD data, the present CFD methodology can provide good prediction of the global field quantities of a propeller. The proposed methodology will be applied to the upcoming work on free running simulations of marine vessels. This current study can be extended to assess and validate the effect of a non-uniform fluid flow (e.g. rotating flows) and the presence of the hull on the propeller performance.

PART 3B: Body Force Propeller

This sub-chapter presents brief information on a body force propeller.

3.5. Governing Equations

Given the propulsion performance characteristics (K_T and K_Q as a function of J), the free running simulations utilised a body force propeller to reduce the computational time and resource. The model used an actuator disk representing the actual propeller geometry with a simple cylindrical shape that has identical diameter and thickness. The model prescribed the axial and theta momentum sources on the disk using the predetermined K_T and K_Q, and distributed based on the radial circulation distributions presented by Hough and Ordway (1964). The axial (fb_x) and theta (fb_θ) momentum source distributions are given as:

$$fb_x = A_x r^* \sqrt{1-r^*} \tag{3-2}$$

$$fb_\theta = A_\theta \frac{r^* \sqrt{1-r^*}}{(1-Y_h)r^* + Y_h} \tag{3-3}$$

where,

$$A_x = \frac{C_T}{\Delta x} \frac{105}{16(4+3Y_h)(1-Y_h)} \tag{3-4}$$

$$A_\theta = \frac{K_Q}{\Delta x J^2} \frac{105}{\pi(4+3Y_h)(1-Y_h)} \tag{3-5}$$

$$r^* = \frac{(y-Y_h)}{(1-Y_h)} \tag{3-6}$$

$$Y_h = \frac{R_h}{R_p} \tag{3-7}$$

R_p and R_h are the propeller and hub radii, and Δx is axial extension of the propeller. C_T is defined as $K_T \pi / 8J^2$. Note that this model neglects the tangential velocities and hence the radial source term is assumed zero.

3.6. Momentum Source Distribution

An example of the source distributions over the propeller radius is shown in Figure 3-8. The propeller has a radius of 0.125m with a hub radius of 0.02m. The both source components are zero in the hub and tip, and varied along the propeller radius.

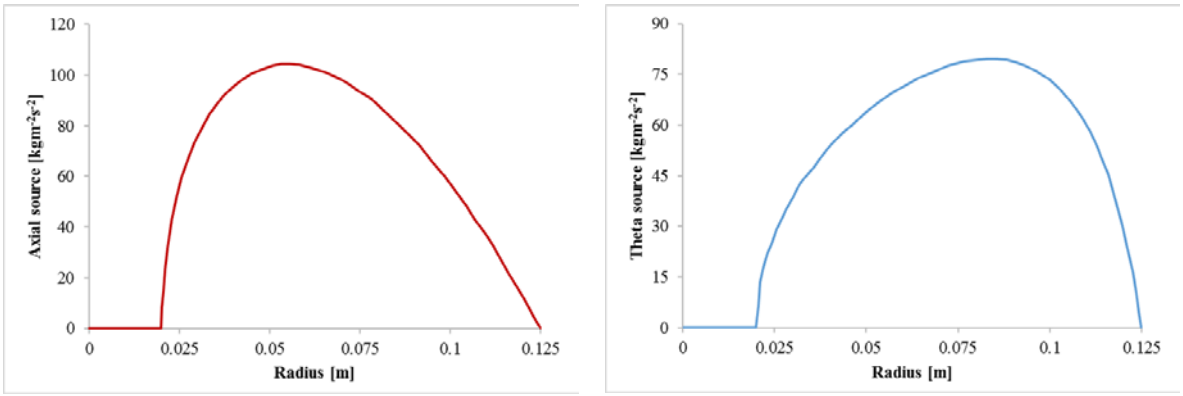

Figure 3-8: An example of the axial and theta source distributions over the propeller radius

[Page intentionally left blank]

Chapter 4: Straight Line Manoeuvring Simulation

This chapter has been published in the Proceedings of the Pacific 2015 International Maritime Conference. The citation for the research article is:

Kim, H., Leong, Z.Q., Ranmuthugala, D., Forrest, A. & Chin, C., 2015, 'CFD modelling and validation of an Underwater Vehicle undergoing variable accelerations', *Proceedings of the Pacific 2015 International Maritime Conference*, 6-8 October 2015, Glebe Island, Australia.

[Page intentionally left blank]

Chapter 5: Six-DOF Free Running Simulation

This chapter consists of two sub-chapters:

Part 5A- Straight Line and Steady Turning Manoeuvres

Part 5B- Zig-zag manoeuvre

[Page intentionally left blank]

PART 5A: Straight Line and Steady Turning Manoeuvres

This sub-chapter has been published in the Journal of Ocean Engineering. The citation for the research article is:

Kim, H., Ranmuthugala, D., Leong, Z.Q., & Chin, C. 2018, 'Six-DOF simulations of an underwater vehicle undergoing straight line and steady turning manoeuvres', *Ocean engineering*.

Abstract

This paper reports on numerical simulations conducted on an underwater vehicle for six-degrees of freedom (6-DOF) free running manoeuvres using Computational Fluid Dynamics (CFD). The CFD manoeuvring trials (straight line and steady turning manoeuvres) were conducted using a model-scaled BB2 submarine with movable control planes and a body force propeller represented by an actuator disk incorporating predetermined propulsion properties. The propulsion properties were obtained from captive self-propulsion simulation adopting the actual BB2 propeller. The free running simulations were validated against experimental data. The results showed that the 6-DOF CFD simulations are capable of predicting the BB2 manoeuvring characteristics with good agreement against the experimental data. The 6-DOF manoeuvring simulations carried out allow for the unsteady viscosity effects, which is usually a limitation of the traditional coefficient-based prediction method. The simulations will enable accurate determination of the vehicle's manoeuvring characteristics, which are essential for the control system design and its safe operating envelope.

Keywords: Computational Fluid Dynamics, underwater vehicles, free running model, 6-Degrees of Freedom manoeuvring simulation, movable control planes

5.1. Introduction

Underwater vehicles require control systems that can adjust the control planes of the vehicle in order to carry out course changes and maintain its intended course during a mission. The control signals directed to the various control planes are influenced by the vehicle's manoeuvring characteristics. Thus, an accurate determination of the manoeuvring characteristics is essential to ensure that the control system of the vehicle is adequately designed to maintain its desired trajectory for each manoeuvre during a mission or operation. The manoeuvring characteristics can be examined using numerical techniques, experimental programmes, or a combination of both. The former includes two approaches, i.e. coefficient-based or physics-based methods. The coefficient-based method uses a mathematical model that implements motion equations (Gertler & Hagen, 1967; Feldman, 1979) incorporating hydrodynamic coefficients. This method is usually adopted because of its rapid simulation time with predefined, constant, coefficients. However, it is limited in its capability to carry out accurate manoeuvring predictions owing to its inability to capture unsteady viscous effects, specifically cross flow and vorticity (Bettle, 2013). To overcome these limitations and increase accuracy in the determination of manoeuvring characteristics, the physics-based method is proposed in this study. This involves a free running test of a vehicle moving in response to its control planes, propeller, and the environment (See Figure 5-1).

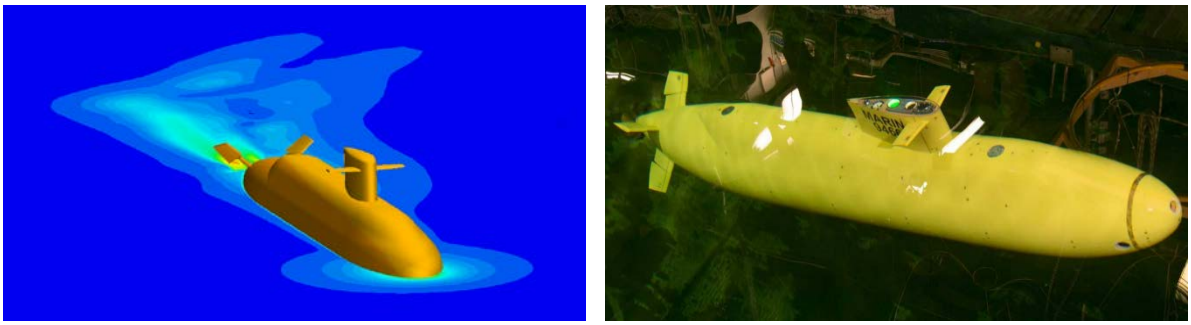

(a) (b)

Figure 5-1: Example of free running model scale submarine: (a) CFD simulation model of the BB2 submarine (Australian Maritime College), (b) BB2 free running physical model undergoing testing at MARIN (Overpelt et al., 2015)

In the past, free running tests of underwater vehicles have often been carried out experimentally using physical models operated in controlled environments (Itard, 1999; Issac et al., 2007; Jun

et al., 2009; and Overpelt et al., 2015). However, they have limitations due to cost and the need for specialised equipment and facilities. With increasing capabilities in Computational Fluid Dynamics (CFD) and High Performance Computing (HPC), CFD based free running tests are becoming more affordable and well suited to supplement experimental studies, although validation may yet require experimental results.

Chase (2012) conducted a 1-DOF (Degrees of Freedom) free running CFD simulation of the fully appended SUBOFF (Groves et al., 1989) generic submarine hull with fixed control planes and a rotating propeller. The CFD results were validated against experimental self-propulsion test data with good agreement in terms of the propulsion properties (i.e. thrust coefficient, K_T; torque coefficient, K_Q and propeller efficiency, η) at a vehicle speed of 1.75 m/s. However, the work was limited to computing the vehicle`s trajectory, speeds and accelerations to 1DOF due to the intensive computational cost involved with modelling a rotating propeller. Chase suggested replacing the rotating propeller with a body force propeller model that would significantly reduce the simulation time.

Bettle (2013) developed a 6-DOF submarine simulation that involved an Unsteady Reynolds Averaged Navier Stokes (URANS) solver coupled with the submarine equations of motion for the SUBOFF generic submarine. The hydrodynamic characteristics of the propeller and controls were represented by force vectors to reduce the computational cost of the model. The capability of the Bettle's model was evaluated for an emergency rising manoeuvre, with the results compared against predictions from a coefficient-based simulation. The largest difference was found to be a 10 % increase in pitch angle. Bettle attributed this discrepancy to the coefficient-based model incorporating rotary hydrodynamic coefficients that were calculated using semi-empirical methods. As future work to verify the discrepancy, Bettle suggested the 6-DOF URANS simulations should include actual control planes and propeller, and compared against free running experimental measurements if available.

Coe (2013) developed a 6-DOF CFD free running model for a General Purpose AUV (GPAUV). The study involved URANS simulations coupled with a 6-DOF Rigid Body Dynamics (RBD) model using the commercial CFD package, Star-CCM+. The deflection of the control planes was realised by an overset grid technique in conjuction with a body force propeller. The body force propeller involved an actuator disk which produces thrust based on

the known propeller performance curves. Coe stated that the poor agreement in trajectories and velocities from the comparison of free running simulations against free running experimental measurements were not conclusive. The poor agreement is mainly due to issues on the experimental trials involving unexplained static offset of rudders (e.g. approximately four degrees offset during the zig-zag manoeuvre). Another possible cause for the discrepancy was that the simulations ignored the D-rings which were affixed to the hull to facilitate deployment and recovery of the vehicle. Coe suggested further work on additional free running experimental measurements for further validation of the CFD results; for example performing a steady turning manoeuvre to provide additional insight into the sources of discrepancies between CFD and experimental results.

The aim of this study is to investigate CFD capabilities as a tool to conduct the 6-DOF free running manoeuvring simulations of a fully appended underwater vehicle. It extends upon the works by Bettle (2013) and Coe (2013) by adopting movable control planes and the actuator disk propeller in the 6-DOF free running simulation using Star-CCM+. The 6-DOF simulation is physics-based and is able to describe the accelerations of the vehicle with respect to the forces and moments due to weight, buoyancy and the hydrodynamic forces. The actuator disk propeller is described using the propulsion characteristics obtained through the captive self-propulsion test included in this study. The credibility of the CFD free running simulation results was established through validation against experimental data provided by Overpelt et al. (2015). The latter experiments were conducted by MARIN at the Seakeeping and Manoeuvring Basin (SMB) in Wageningen, Netherlands. The basin filled with fresh water having a density of 1000 kg/m^3. The experimental data was given for full scale in salt water (1025 kg/m^3), which required scaling based on Froude scaling laws with a model scale factor (λ) of 18.348 (Overpelt et al., 2015). The aft control planes employed a 'X' form configuration consisted of four control planes moving independently to control the horizontal and vertical motions of the vehicle. The individual angle of the planes were commanded by an autopilot that used a Proportional-Derivative (PD) controller with a coupled proportional and derivative control parameter for translations and rotations (Overpelt et al., 2015).

The CFD model and its methodology developed in this study can be used by underwater vehicle designers to carry out 6-DOF manoeuvring simulations for various vehicle designs, configurations and missions. Addressing the limitation of the coefficient-based prediction, in

accounting for the non-linear characteristics of the vehicle due to unsteady viscosity effects, the 6-DOF physics-based simulation will enable the designers to accurately determine a vehicle's manoeuvring characteristics for control system design and its safe operational limits.

5.2. Methodology

5.2.1. Investigation Programme

This study utilised the BB2 generic submarine geometry (Overpelt et al., 2015), which represents a typical conventional (SSK) submarine. The design was derived from hull form introduced by Joubert (2006), and the BB2 hull has a full scale length of 70.2 m. The BB2 submarine consists of a sail, x-configuration stern control planes, and a hull with a casing on top. This study employed the model scale BB2 geometry (Figure 5-2) based on Froude scaling laws with a scale factor (λ) of 18.348, giving the model a length of 3.826m.

(a)

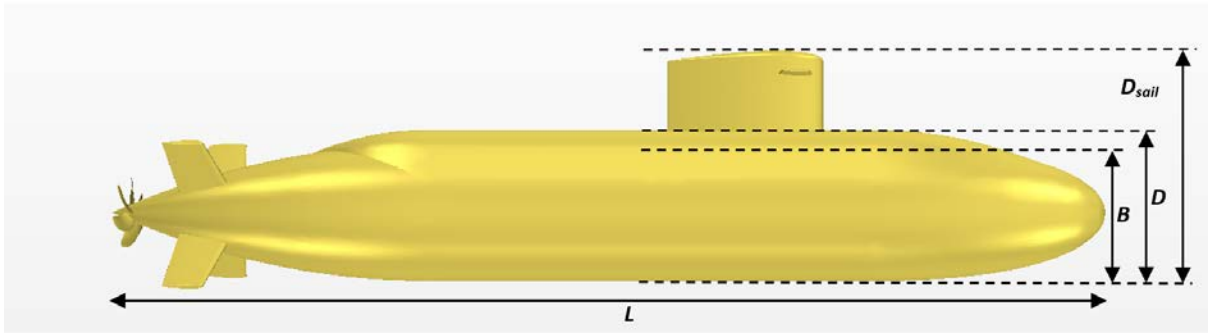

(b)

Figure 5-2: Model scale BB2: (a) MARIN physical model (Overpelt et al., 2015) and (b) CFD. The dimensions are: Length (L) = 3.826 m; Breadth (B) = 0.523 m; Depth from deck (D) = 0.578 m; Depth from sail tip (D_{sail}) = 0.883 m

The submarine motion is described through a 6-DOF body coordinate frame of reference (see Figure 5-3), in which the origin (O) is located at the Centre of Gravity (*CG*) with the positive directions along the *x*, *y* and *z* axes being forward, starboard, and vertically downwards respectively. The motion variables are listed in Table 5-1.

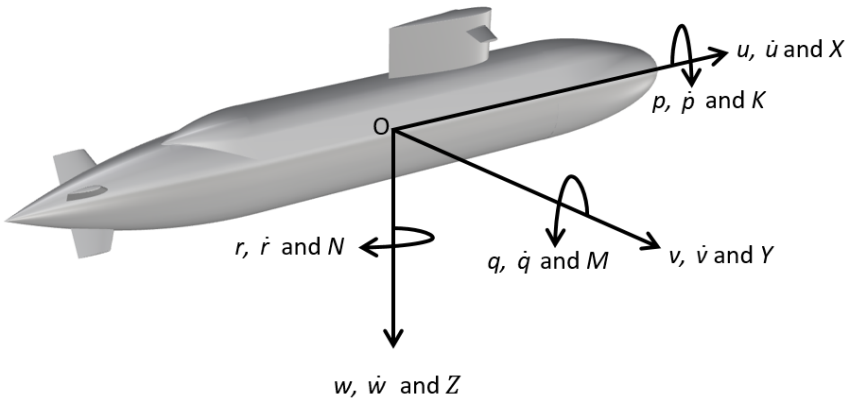

Figure 5-3: Body fixed coordinate with the origin (O) located at the Centre of Gravity (*CG*)

Table 5-1: Motion variables in a body coordinate frame of reference

Motion	**Forces [N] and moments [Nm]**	**Linear [m] and angular [degrees] displacements**	**Linear [m/s] and angular [degrees/s] velocities**	**Linear [m/s^2] and angular [degrees/s^2] accelerations**
Surge	*X*	x	u	u̇
Sway	*Y*	y	v	v̇
Heave	*Z*	z	z	ẇ
Roll	*K*	ϕ	p	ṗ
Pitch	*M*	θ	q	q̇
Yaw	*N*	ψ	r	ṙ

The current CFD model ensures that the Longitudinal Centre of Buoyancy (*LCB*) is placed at the same position as the Longitudinal Centre of Gravity (*LCG*), and the vertical stability lever

was set at 0.022 m with the *CG* below the Centre of Buoyancy (*CB*). This gives a vertical stability lever of 0.0057 × *L*, which replicated the physical model. The details of the mass properties are presented in Table 5-2.

Table 5-2: Mass properties of the scaled BB2 submarine by a factor of 18.348; the longitudinal and vertical *CG* was measured from the front nose tip and the keel, and the moments of inertia (i.e. *Ixx*, *Iyy* and *Izz*) are about the *CG*.

Property	**Value**	**Unit**
Length (*L*)	3.826	m
LCG (from the front nose tip)	1.76	m
LCB (from the front nose tip)	1.76	m
VCG (from the keel)	0.267	m
VCB (from the keel)	0.289	m
Mass (*m*)	703.976	kg
Ixx (about the *CG*)	30.849	kgm^2
Iyy (about the *CG*)	665.448	kgm^2
Izz (about the *CG*)	665.229	kgm^2

Straight line and steady turning manoeuvres CFD free running tests were calculated at the same depth condition (i.e. 2.5 m depth from the water surface in a 5 m deep test basin) as the experimental fluid dynamics (EFD) cases. The straight line case involved three vehicle speeds (0.73, 0.97, and 1.19 m/s) and the steady turning case involved two effective rudder angles (20 and 30 degrees) at a nominal speed of approximately 1.19 m/s, which is equivalent to a Reynolds number (*Re*) of 5.2×10^6. The depth and pitch were controlled by an autopilot to maintain the desired vehicle stability. All cases adopted movable control planes in conjunction with a body force propeller using an actuator disk, which mimicked the propeller propulsion properties obtained from a captive self-propulsion test (see Section in 5.2.3 (a)). Note that sail planes were kept at zero degrees for all manoeuvres. A summary of the simulation cases is given in Table 5-3. Validation was carried out against experimental measurements provided by Overpelt et al. (2015) .

Table 5-3: Simulation cases with parameters

Manoeuvres	**Effective rudder angle [degrees]**	**Speed [m/s]**
Straight line	0	0.73, 0.97 and 1.19
Steady turning	20 and 30	1.19

The 'X' stern configuration consisted of four control planes moving independently to maintain translational and rotational stability in 6-DOF throughout the course of the manoeuvres. The autopilot commanded effective rudder (δ_r) and effective sternplane (δ_s) angles, with individual plane angles ($\delta_{\text{up port}}$, $\delta_{\text{down port}}$, $\delta_{\text{up starboard}}$ and $\delta_{\text{down starboard}}$) calculated using Equations (5-1) to (5-4) based on the right hand rule with the thumb pointing away from the body (Overpelt et al. 2015). Note that the maximum plane angle for each of the control planes was limited to 30 degrees.

$$\delta_{up\ port} = \delta_r + \delta_s \tag{5-1}$$

$$\delta_{up\ starboard} = \delta_r - \delta_s \tag{5-2}$$

$$\delta_{down\ starboard} = -\delta_r - \delta_s \tag{5-3}$$

$$\delta_{down\ port} = -\delta_r + \delta_s \tag{5-4}$$

Thus, the effective rudder and sternplane angles were be calculated as,

$$\delta_r = \frac{\delta_{up\ port} - \delta_{down\ port} + \delta_{up\ starboard} - \delta_{down\ starboard}}{4} \tag{5-5}$$

$$\delta_s = \frac{\delta_{up\ port} + \delta_{down\ port} - \delta_{up\ starboard} - \delta_{down\ starboard}}{4} \tag{5-6}$$

The autopilot and feedback controller utilised a Proportional-Derivative (PD) controller with associated proportional and differential control parameters for translations and rotations (see Table 5-4), as used in the experiment (Overpelt et al., 2015).

Table 5-4: Autopilot PD parameters (Overpelt et al., 2015) for the scaled BB2 submarine by a factor of 18.348.

Description	***P* (Proportional parameter)**		***D* (Derivative parameter)**	
	Symbol	**Value**	**Symbol**	**Value**
Translation in *y* direction	P_y	18.3 [degrees/m]	D_y	0 [degrees/(m/s)]
Translation in *z* direction	P_z	-55.04 [degrees/m]	D_z	-12.85 [degrees/(m/s)]
Rotation about *y* axis	P_θ	3 [degrees/degree]	D_θ	0.7 [degrees/(degree/s)]
Rotation about *z* axis	P_φ	3 [degrees/degree]	D_φ	2.85 [degrees/(degree/s)]

The equations for the PD controller are as follows (Overpelt et al., 2015):

$$\delta_r(t) = P_z e(t) + D_z \frac{de(t)}{dt} + P_\theta e(t) + D_\theta \frac{de(t)}{dt} \tag{5-7}$$

$$\delta_S(t) = P_y e(t) + D_y \frac{de(t)}{dt} + P_\varphi e(t) + D_\varphi \frac{de(t)}{dt} \tag{5-8}$$

where $e(t) = e_{desire} - e_{current}$ and $\frac{de(t)}{dt} = \frac{e(t)_{current} - e(t)_{previous}}{t_{current} - t_{previous}}$.

5.2.2. Numerical Strategy

a. Numerical settings

The CFD simulations utilised URANS with turbulence model using the Elliptic blending reynolds stress model (CD-adapco, 2015), coupled to 6-DOF RBD (Kim et al., 2015b). The URANS equations solved the flow field for prediction of the vehicle's hydrodynamics. This was then applied to compute the vehicle's resulting motion using the RBD equations with linear

and angular momentum solvers for translation and rotation of the vehicle defined as a rigid body with its mass properties as referred in Table 5-2.

All simulations in this study were performed under transient conditions to investigate the behaviour of the vehicle in the time domain. The fresh water, with the same density as measured during the experiments (i.e. 1000 kg/m^3), was specified for the single-phase fluid, which was assumed to be incompressible and isothermic. To minimise numerical diffusion, a second-order upwind scheme, with a maximum of ten inner iteration loops for convergence per time-step, was employed in the simulations. Courant-Friedrichs-Lewy (CFL) numbers were maintained below 6 in the majority of the computational domain throughout the simulations. Note that a segregated flow model is used with a predictor-corrector approach to link between the momentum and continuity equations.

b. Grid model

The type and element size of the grid play an important role in the computation as these influence the convergence and accuracy of the simulated results. This study used an unstructured hybrid polyhedral for its ability to represent the complex geometry without excessively dense grid and high time demand. Inflation layers consisting of polyhedral-prisms were applied on the surface of the vehicle to capture its boundary layer. The free running simulations are extremely sensitive to the grid resolution on the vehicle's geometry as inaccurate geometrical representation leads to errors in prediction of the vehicle's *CB* and forces and moments on the vehicle (CD-adapco, 2015). Thus, it is important to ensure that grid resolution is sufficient to represent the geometry. In this study, the grid resolution error of the BB2 geometry was maintained at less than 0.02%.

5.2.3. Free Running Simulation Setup

The free running simulation model involved the vehicle operating with movable control planes and a body force propeller. The latter is described using the propeller performance characteristics (i.e. K_T , K_Q and η) that were obtained from the captive self-propulsion

simulation, which was carried out using CFD and employing the propeller geometry used in the experiment (Overpelt et al., 2015).

a. Captive self-propulsion model

Model setup

Figure 5-4 shows the grid for a captive self-propulsion model, with the local refinement on the aft control planes and the propeller tip, leading and trailing edges, and blade surface regions, shown in Figure 5-4 (b), and the actual experimental model propeller and the aft control planes, shown in Figure 5-4 (c). The grid size on the interface between the propeller and the surrounding fluid flow was prescribed to rotate one grid face per degree based on a maximum applied rotational speed employed during the experiments (i.e. 266 rpm). Additional grid refinement was carried out on the far field region shown in Figure 5-4 (a), as variation of the physical quantities in these regions would be comparatively high. The total boundary layer thickness and its distribution was achieved through prescribing the first layer thickness reflected by the y^+ value, and were estimated based on the calculations presented previously by the authors (Kim et al., 2015b). The y^+ values were less than 1 for the hull to adequately resolve the boundary layer, and a minimum of 30 for the propeller to allow the first node from the adjacent hull surface to be placed in the log-wall region for use with a wall function. The boundary conditions applied were a velocity inlet forward of the vehicle with zero velocity, pressure outlets at the sides around the vehicle, pressure outlet at the boundary aft of the vehicle, and no-slip walls on the vehicle (see Figure 5-7 (a)).

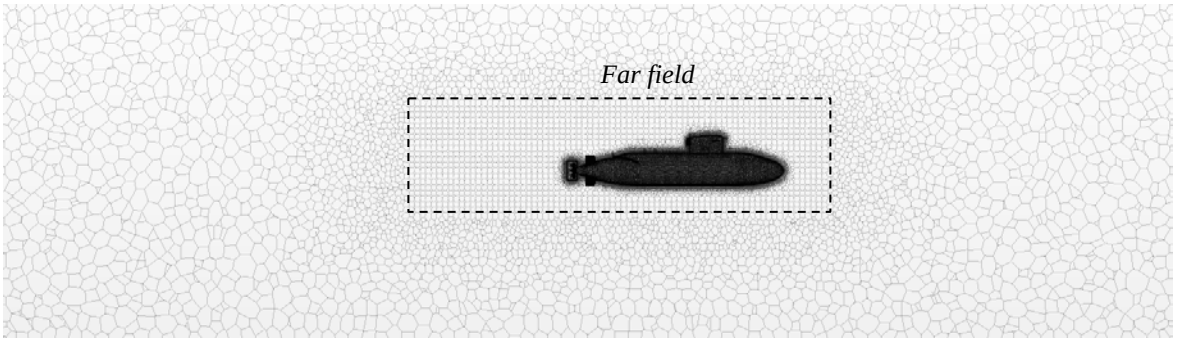

(a)

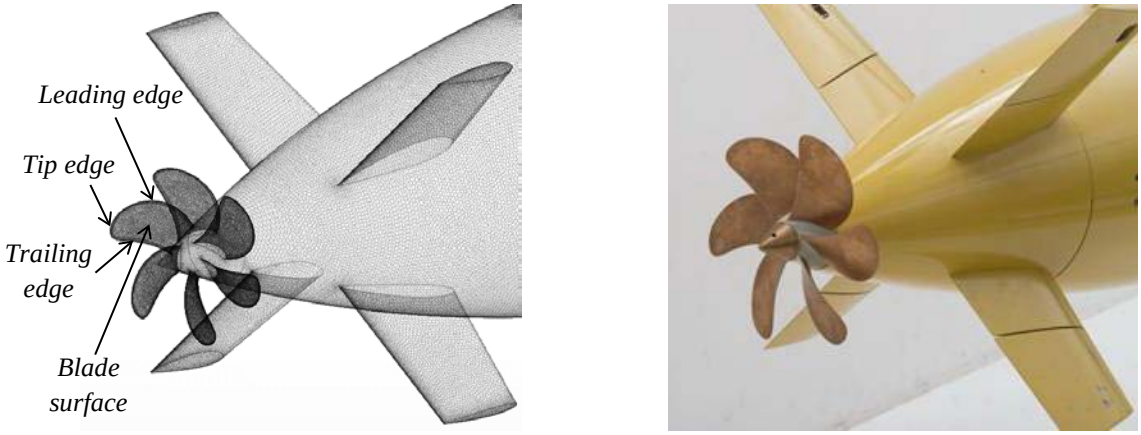

(b) (c)

Figure 5-4: (a) Unstructured hybrid polyhedral grid on $y = 0$ symmetry plane for the captive self-propulsion simulations, (b) CFD discretised propeller and (c) physical propeller model (Ovepelt et al., 2015).

Discretisation studies

To confirm that the grid providing fluid prediction is independent of the grid discretisation resolution, a grid dependence study was performed for the vehicle in the captive self-propulsion condition.

Table 5-5: Grid dependence study of the discretised propeller and hull, showing the percentage difference to the very fine grid level (4.28 and 19.10 million cells for the discretised propeller and hull, respectively) at the operating propeller revolution of 266 rpm and the maximum operational speed of 1.4 m/s.

	Propeller			**Hull**	
Grid level	**Cells [Million]**	**Thrust difference to Very fine grid [%]**	**Torque difference to Very fine grid [%]**	**Cells [Million]**	***X* force difference to Very fine grid [%]**
Coarse	2.98	1.88	1.19	6.34	2.16
Medium	4.01	1.74	1.08	9.21	1.82
Fine	4.28	0.38	0.11	14.78	0.76
Very fine	4.45	-	-	19.10	-

The thrust and torque of the propeller and the force in the *x* direction on the hull were examined for a series of grid levels from coarse to very fine. Table 5-5 shows the percentage difference of each grid level compared to the finest grid at the maximum operating propeller revolution of 266 rpm and forward speed of 1.4 m/s. It is seen that, at the fine grid level, the predictions of thrust, torque, and *X* force were within 1 % of the finest (very fine) grid investigated. As a conservative measure, the fine grid configuration was adopted for the captive self-propulsion simulations.

The temporal discretisation was examined to ensure sufficient time resolution to capture the 3D transient flow fields around the propeller as well as the vehicle. A time-step dependence study was carried out at various time-steps as shown in Table 5-6. It also shows the percentage difference of the thrust, torque, and force *X* between the applied time-step and the smallest time-step (0.0005 s, corresponding to 0.8 degrees of propeller rotation per time-step). For the propeller, it is seen that at the 0.0015 s time-step, the thrust and torque predictions were within 1 % of the smallest time-step investigated. For the hull, a time step of 0.025 s or smaller resulted in the *X* force being predicted within 1 % of the smallest time-step. As a conservative measure, the time-step of 0.0015 s was utilised for the self-propulsion simulations.

Table 5-6: Time-step dependence study, showing the percentage difference to the smallest time-step (0.0005 s, corresponding to 0.8 degrees/s per time-step) for the thrust, torque and *X* force on the propeller and hull at a propeller rotation of 266 rpm and inflow velocity of 1.4 m/s.

	Propeller			**Hull**
Time-step [s]	**Revolution speed per each time-step [degrees/s]**	**Thrust difference to the smallest time-step [%]**	**Torque difference to the smallest time-step [%]**	***X* force difference to the smallest time-step [%]**
0.025	39.897	4.56	3.89	0.25
0.005	7.979	2.31	1.22	0.16
0.0015	2.394	0.33	0.22	0.09
0.0005	0.8	-	-	-

Propeller performance characteristics

The performance characteristics of the propeller were predicted from the captive self-propulsion tests with a constant rotational speed of 266 rpm and varying freestream velocity at the inlet (see Figure 5-5). The advance coefficients (J) were computed based on the average velocities measured at a plane placed 0.136 m forward of the propeller origin (see Figure 5-7). The predicted performance properties were fed into the actuator disk employed in the free running simulations.

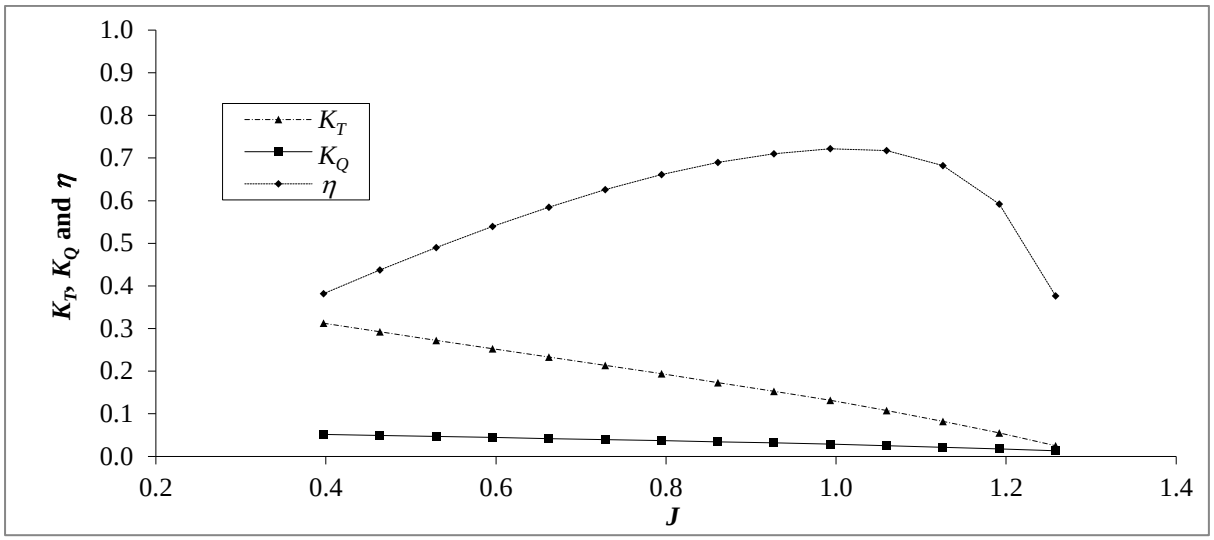

Figure 5-5: Propeller performance properties of the BB2 propeller under captive self-propulsion condition with a constant rotational speed of 266 rpm. The advance coefficients (J) were computed based on the average velocities measured at a plane placed 0.136 m forward of the propeller origin.

b. 6-DOF free running model

The fine grid configuration (shown in Figure 5-6) was selected for the free running simulation model. The separate grids for the background fluid domain and control planes were connected using the overset interface (see Figure 5-7). The additional grid refinement on the propeller wake region shown in Figure 5-7 was prescribed for effective use of the actuator disk (CD-adapco, 2015).

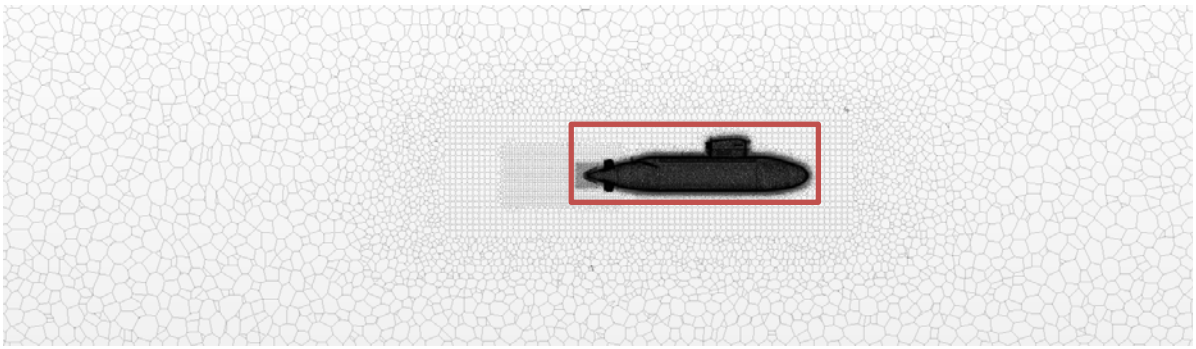

(a)

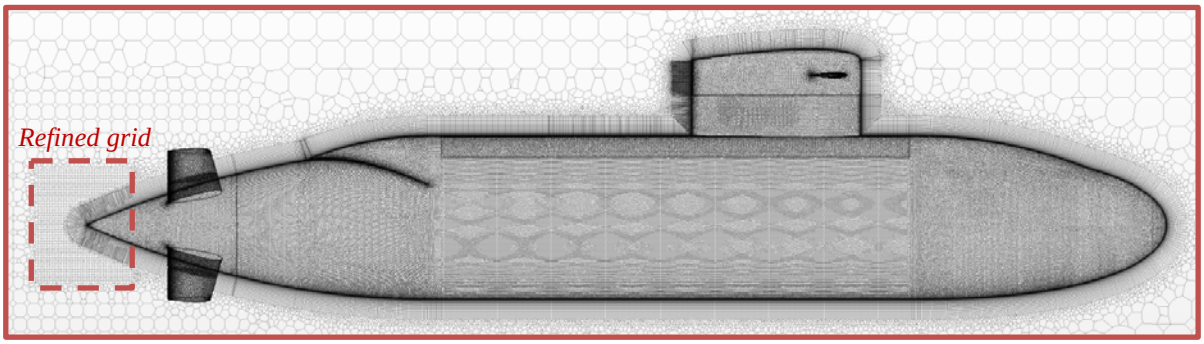

(b)

Figure 5-6: (a) Free running model grid adopted (fine grid level, 14 million cells) on y=0 symmetry plane and (b) magnified view showing the grid refinement around the propeller wake region.

The free running vehicle motion was applied to the complete grid domain, including the vehicle and the background regions, while keeping the fluid stationary. This prevented the degradation of the grid quality that may otherwise have occurred as a result of grid deformation in order to accommodate the vehicle's motion. Similarly, the boundary conditions led to a reduction in the interference owing to the proximity of the vehicle to the fluid domain boundaries, allowing a reduction of the fluid domain size (Kim et al., 2015a). The applied boundary conditions (see Figure 5-7) were as follows:

- inlet: velocity inlet with zero velocity at the inlet,
- outlet: zero Pa pressure outlet at the sides with 0.05 turbulence intensity and viscosity ratio (μ_t/μ) of 10, and
- wall: no-slip wall on the vehicle with zero relative fluid velocity tangential to the vehicle`s surface.

The dynamic deflection of the control planes was realised using the overset gridding technique. Figure 5-7 shows the overset interface connecting the background and the overset regions containing the control planes. The overset regions were imposed on the background region and rotated at a rate commanded by the autopilot.

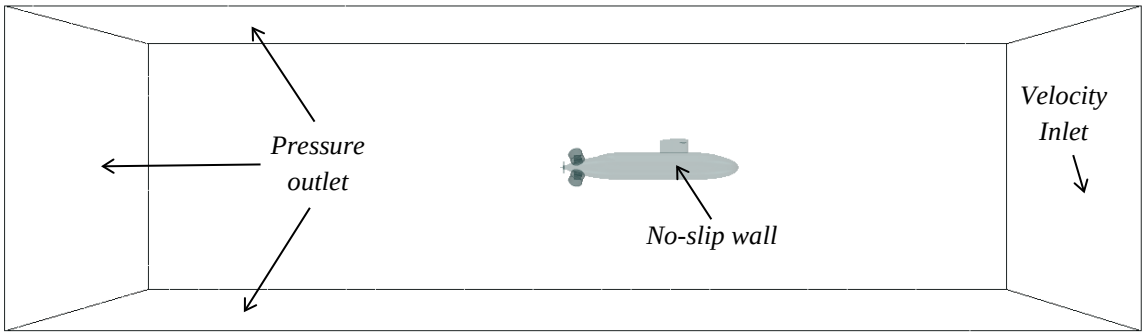

(a)

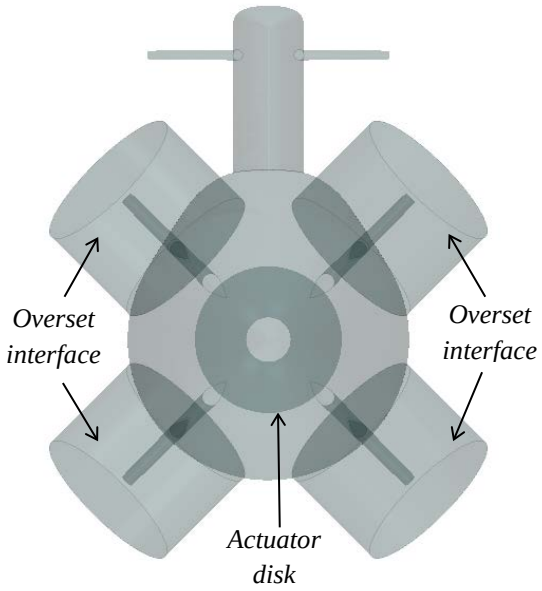

(b)

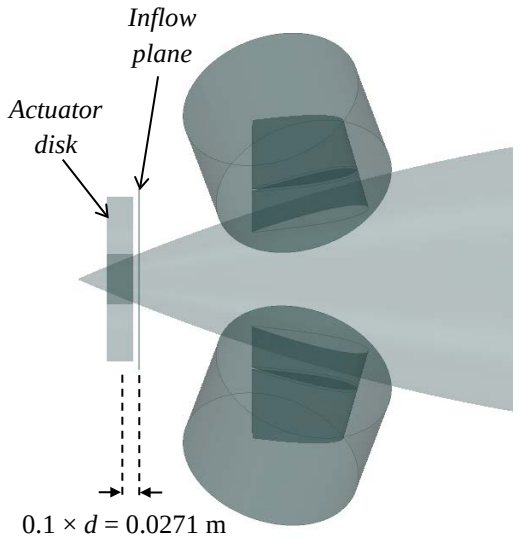

(c)

Figure 5-7: (a) Boundary conditions of the computational domain, (b) view from the astern and (c) magnified view of the stern region showing the positions of the inflow plane (i.e. located forward of the disk origin by 10 % of the disk diameter, *d*, measuring the inflow velocity for computing thrust and torque.

The gap between the planes and the adjacent surface on the hull was around 1 mm in the physical model. However, the overset interface requires at least three layers in the gap (CD-

adapco, 2015), which requires a large number of grid cells with the 1 mm gap. Thus, a 5mm gap was chosen for the present simulation model, resulting in resolution of the gap flow without excessive grid refinement. It was assumed the error due to the altered gap flow is sufficiently small as the increased gap was still small compared to the control plane dimensions.

The actuator disk mimics the effects of a propeller by generating fluid acceleration based on the prescribed magnitude and distribution of fluid momentum sources. The axial and circumferential momentum sources were computed based on the propeller performance properties (K_T and K_Q) with respect to the advance coefficient (J). This was updated simultaneously with an observed inflow velocity at a plane placed forward of the disk origin by 10 % of the disk diameter (d), as shown in Figure 5-7. The distribution of the momentum sources was prescribed in accordance with the Goldstein optimum method (Goldstein, 1929). The method prescribes the distribution of the axial (thrust/swept volume of the disk) and circumferential (torque/swept volume of the disk) momentum components over the radial direction of the actuator disk. For the actuator disk used, the tangential velocities were neglected and hence the radial momentum component was zero (Kim et al., 2015b) . The volume of the disk was determined to be equal to that of the propeller (Phillips et al., 2008) .

5.3. Results and Discussion

5.3.1. Straight Line Manoeuvre

The 6-DOF free running simulations of a straight line manoeuvre was carried out to examine the propeller revolution speeds and thrust forces at the target vehicle's speeds of 0.73, 0.97, and 1.19 m/s, which are equivalent to approximately 6, 8, and 10 knots at full scale, with the vertical control maintaining the depth and pitch angle. The vehicle was initially kept at zero trim and depth at its fixed coordinate, and moved in response to the thrust generated by the disk propeller until the thrust and vehicle resistance were in equilibrium. The simulation results of the thrust and propeller rotational speed were then compared against experimental data. It is noted that the experimental data employed for validation used stern and sail planes for vertical control, while the CFD simulations used only stern planes for vertical control. This was due to the limited availability of experimental data. Given that both the sail and stern planes are mainly

used to maintain the vertical position for a straight line course, the experimental data was still deemed to be acceptable for validating the CFD predictions; proving the vertical position (i.e. depth) was well preserved by the planes.

Figure 5-8 shows the CFD and experimental data of the propeller revolution speed and thrust force at the vehicle's set speeds. The rotational speed and thrust predictions were in very good agreement with the experimental measurements, with differences less than 2 %.

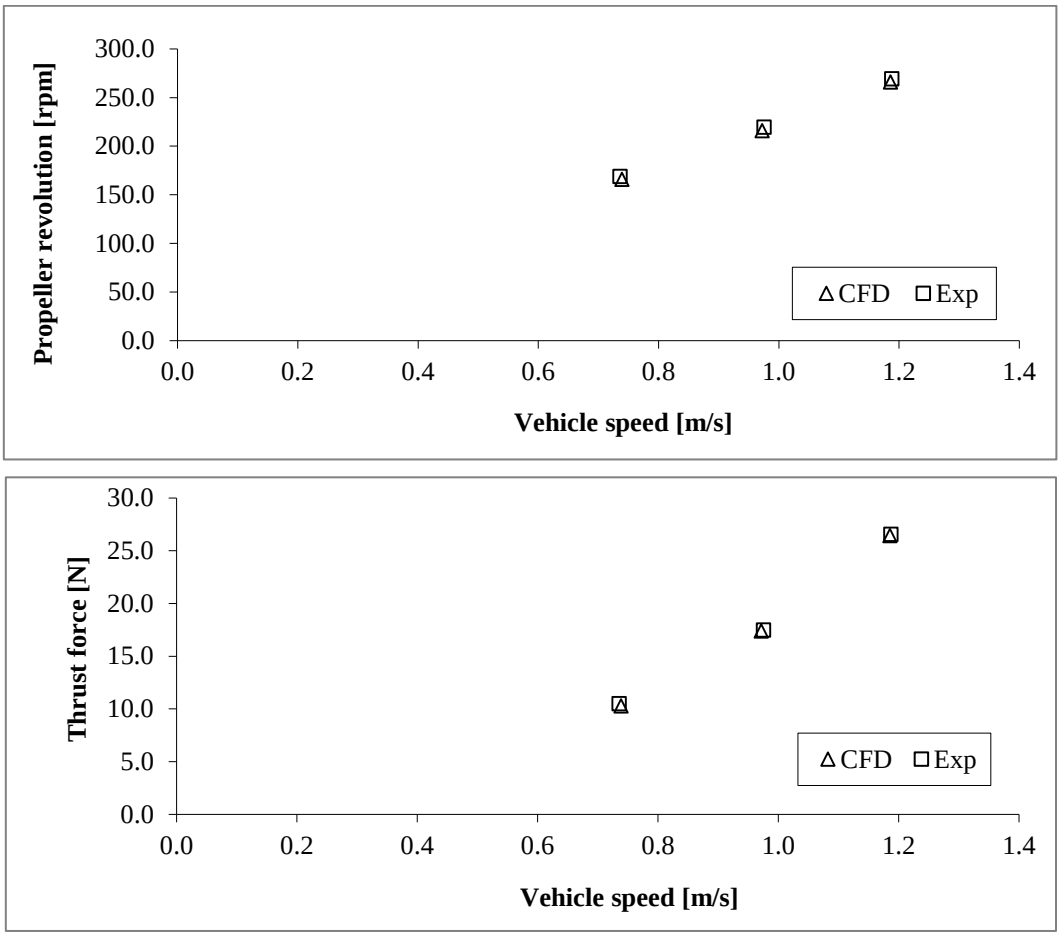

Figure 5-8: CFD and experimental data of the propeller revolution speed and thrust force at the vehicle`s speeds of approximately 0.73, 0.97, and 1.19 m/s.

5.3.2. Steady Turning Manoeuvre

The steady turning manoeuvre involved two effective rudder angles (δ_r = 20 and 30 degrees) executed at a target speed of approximately 1.19 m/s (equivalent to 10 knots at full scale).

When the target speed was reached with a constant propeller rotation, the effective rudder angles were prescribed. The depth and pitch angle were maintained during the manoeuvre by the stern planes with sail planes kept at zero angle. Note that all turns were performed to the port side. The *x-y* trajectories for both turns are shown in Figure 5-9.

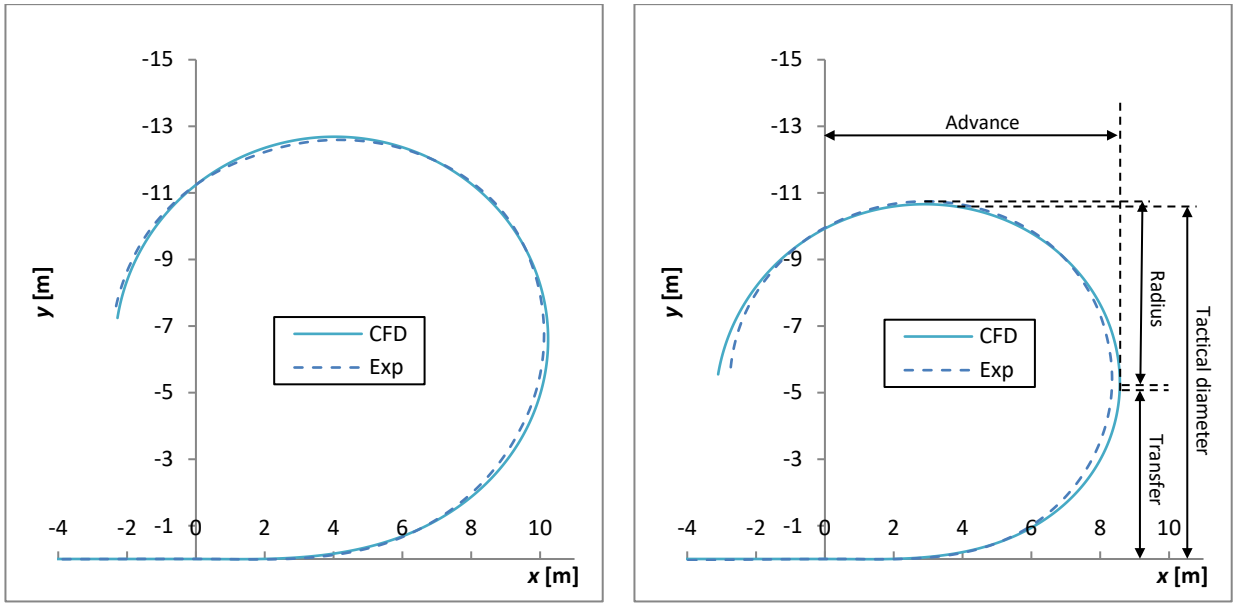

(a) (b)

Figure 5-9: CFD and experiment x-y trajectories for effective rudder angle of (a) 20 degrees and (b) 30 degrees steady turning manoeuvres at an approximate forward speed of 1.19 m/s.

Table 5-7 shows the percentage difference between CFD and EFD for manoeuvring characteristics as per ITTC (2002a), presented in the non-dimensional form based on vehicle length. In both turns, CFD predicted a higher transfer (the perpendicular distance travelled by the CG from the position at start of the turn) at 90 degrees of vehicle`s original heading owing to the greater vehicle`s thrust forces before reaching a steady turn. As the prescribed thrust and torque in the disk propeller are based on a uniform fluid flow, the over-prediction of the transfer may be caused by the disk propeller being unable to accurately predict the loss of thrust force (see Figure 5-10) involving non-symmetric flow on the propeller plane. Overall, the maximum discrepancy was found to be 7.26 %, which still represents a good agreement between CFD and experiments.

Table 5-7 Percentage difference between CFD and experiment for Length (*L*) based non-dimensional manoeuvring characteristics (ITTC, 2002a) for effective rudder angles of 20 and 30 degrees steady turning manoeuvres at a forward speed of approximately 1.19 m/s.

Effective rudder angle		**[1] Advance at 90 degrees [m]**	**[2] Transfer at 90 degrees [m]**	**[3] Tactical diameter at 180 degrees [m]**	**[4] Turning radius at 180 degrees [m]**
20 degrees	CFD	2.65 *L*	1.47 *L*	3.30 *L*	1.60 *L*
	Experiment	2.60 *L*	1.58 *L*	3.28 *L*	1.55 *L*
	Difference [*%*]	2.13	6.87	0.37	3.32
30 degrees	CFD	2.22 *L*	1.14 *L*	2.77 *L*	1.43 *L*
	Experiment	2.17 *L*	1.23 *L*	2.80 *L*	1.42 *L*
	Difference [*%*]	2.22	7.26	1.24	0.71

[1] Advance at 90 degrees: distance travelled by the Centre of Gravity (*CG*) in a direction parallel to the original course at a vehicle`s heading angle of 90 degrees
[2] Transfer at 90 degrees: perpendicular distance travelled by the *CG* at a vehicle`s heading angle of 90 degrees
[3] Tactical diameter at 180 degrees: perpendicular distance travelled by the *CG* at a vehicle`s heading angle of 180 degrees
[4] Turning radius at 180 degrees: radius of the circular arc travelled by the *CG* at a vehicle`s heading angle of 180 degrees

Figure 5-10 shows the time series of the linear velocities and thrust forces for both turns with the effective rudder angle executed at 0 s. The velocities from both the CFD and experimental data followed the trends well with CFD slightly over-predicting *u* by a maximum of 2 % during the steady turning phase of 30 degrees effective rudder turn (see Figure 5-10 (b)). This is attributed to the relatively stronger vortices generated by control planes compared to those of the 20 degrees effective rudder turn. The stronger vortices caused the decrease in thrust force in the experiment, whereas CFD predictions were limited to due to the absence of the propeller blades, and thereby marginally over-predicted *u*. Further free running simulations using a rotating propeller (currently being carried out by the authors) will address this discrepancy, although the simulation will require significantly greater computational time (Stern et al., 2013).

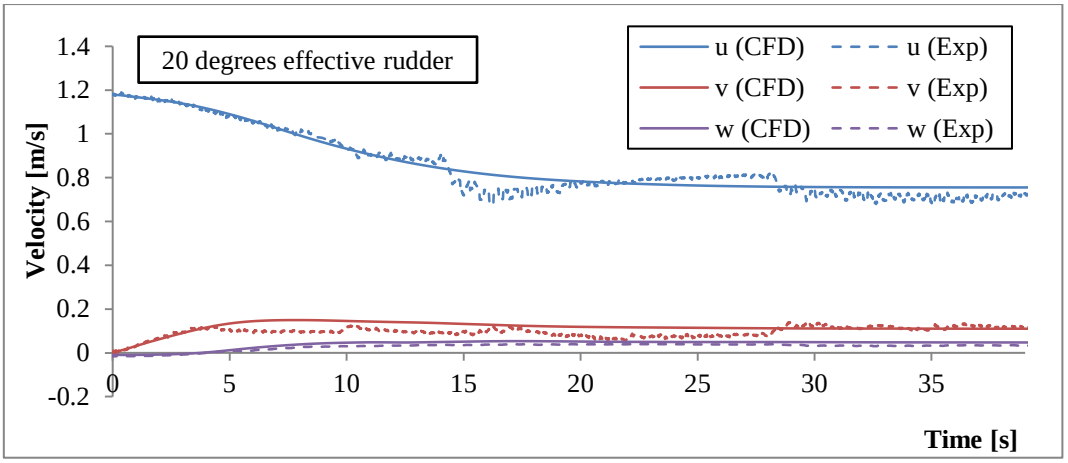
20 degrees effective rudder
u (CFD)
u (Exp)
v (CFD)
v (Exp)
w (CFD)
w (Exp)
Velocity [m/s]
Time [s]

(a)

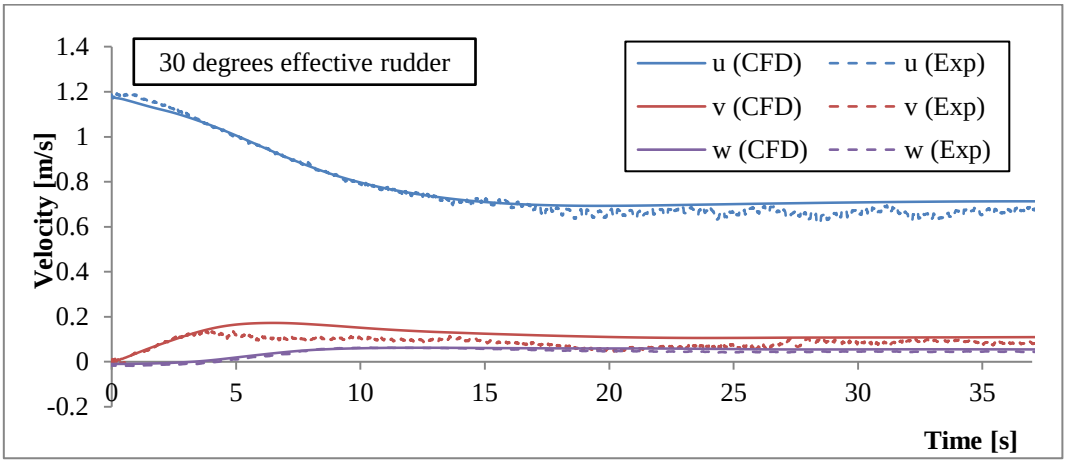
30 degrees effective rudder
u (CFD)
u (Exp)
v (CFD)
v (Exp)
w (CFD)
w (Exp)
Velocity [m/s]
Time [s]

(b)

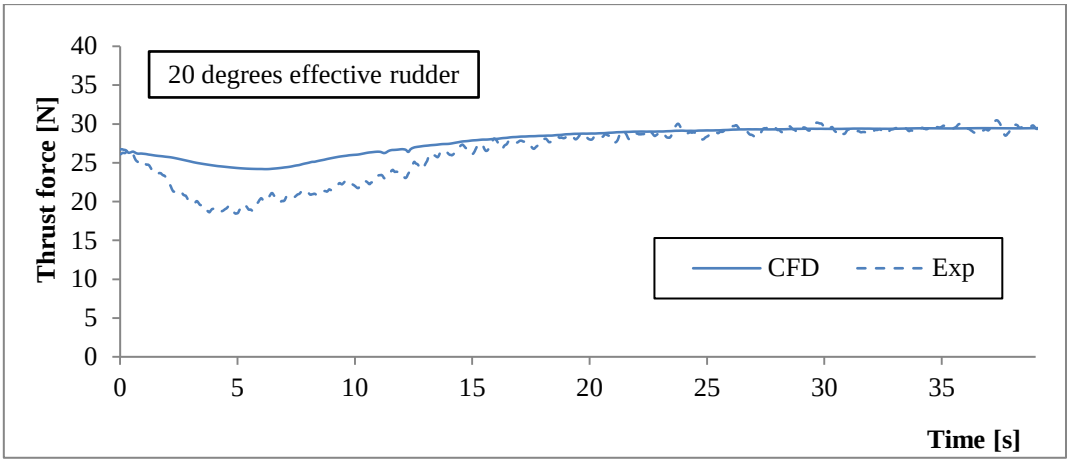
20 degrees effective rudder
CFD
Exp
Thrust force [N]
Time [s]

(c)

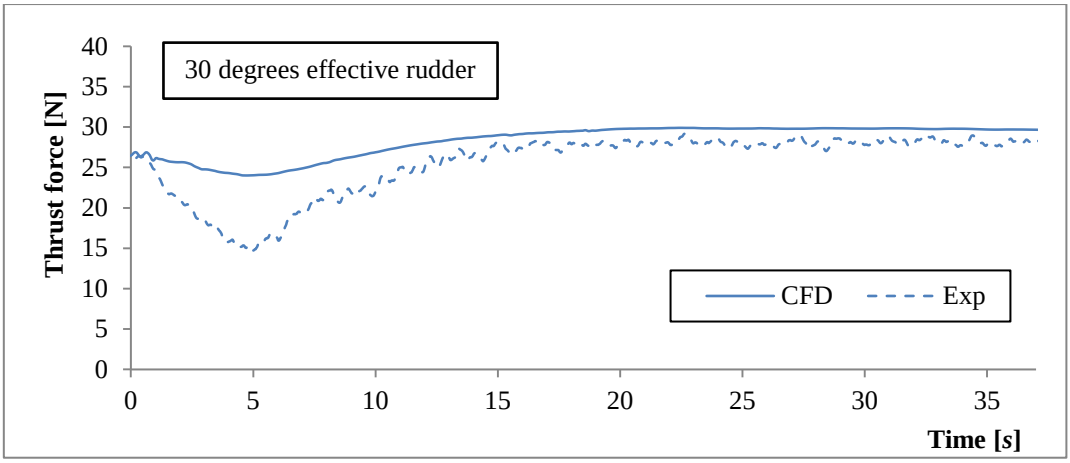

(d)

Figure 5-10: Time history of the (a) and (b) linear velocities and (c) and (d) propeller thrust forces for effective rudder angles of 20 and 30 degrees steady turning manoeuvres at a forward speed of approximately 1.19 m/s.

The time histories of the depths (z) during the turns are shown in Figure 5-11. The discrepancy may be attributed to the coupling nature between pitch angle and depth within the autopilot. For example, the slight over-prediction of pitch angle by about one degree (see Figure 5-12) might cause difference of the predicted depth by 0.05 m. In addition, it is hypothesised that the setting of the desired values for depth and pitch angle for the calculation of the effective stern plane angle (see Equation 8) in the autopilot may cause the discrepancy. The desired values used in the experiment are unknown whereas those in CFD are set to zero (i.e. original depth at start of the manoeuvre), which resulted in a difference in the commanded control plane angles between CFD and experiment (see Figure 5-14). Nevertheless, it is seen in Figure 5-11 that the vehicle's depth gradually decreased and eventually converged to a constant value for both CFD and experiment.

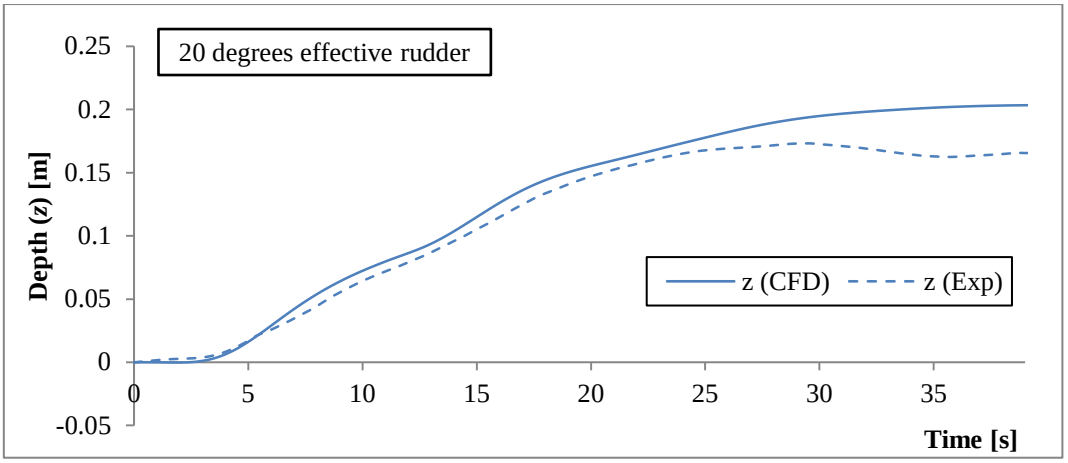

(a)

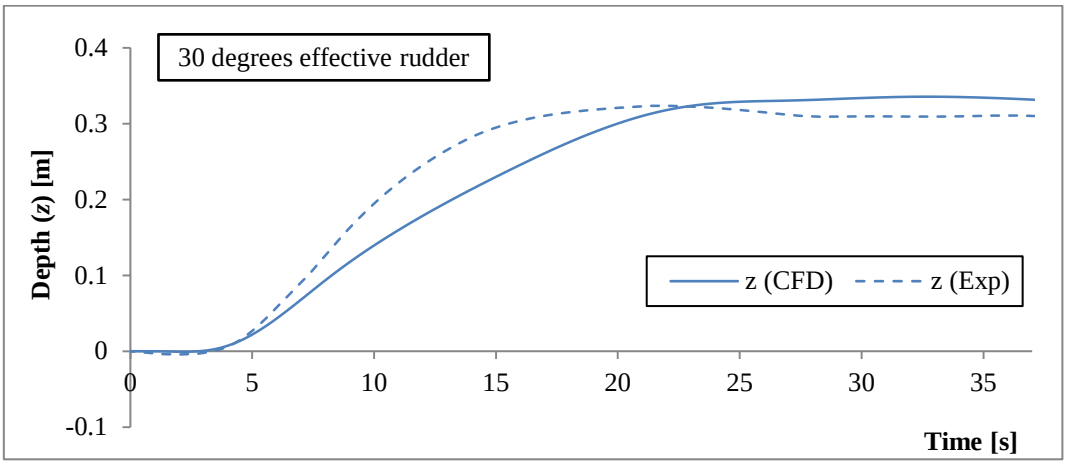

(b)

Figure 5-11: Time history of the depth (*z*) for rudder angle of (a) 20 degrees and (b) 30 degrees steady turning manoeuvres at a forward speed of approximately 1.19 m/s.

A time trace of roll (ϕ) and pitch (θ) angles is shown in Figure 5-12. It is observed that the vehicle had a tendency to pitch bow up when in a steady turn. This is likely attributed to the out-of-plane forces caused by the presence of the sail, resulting in a generation of the downward force on the vehicle`s stern region (Leong et al., 2016). As previously discussed, the discrepancy in pitch angle may be due to the difference in the effective stern plane angle due to the desired values for depth and pitch angle set in the autopilot. Another possible cause of the discrepancy might be a slight difference in *CB* between the CFD and physical models, which might possibly be aggravated by the increase in pressure with depth in experimental testing. The roll angle caused by a reaction to the propeller torque and side forces on the vehicle was predicted to less than a degree discrepancy.

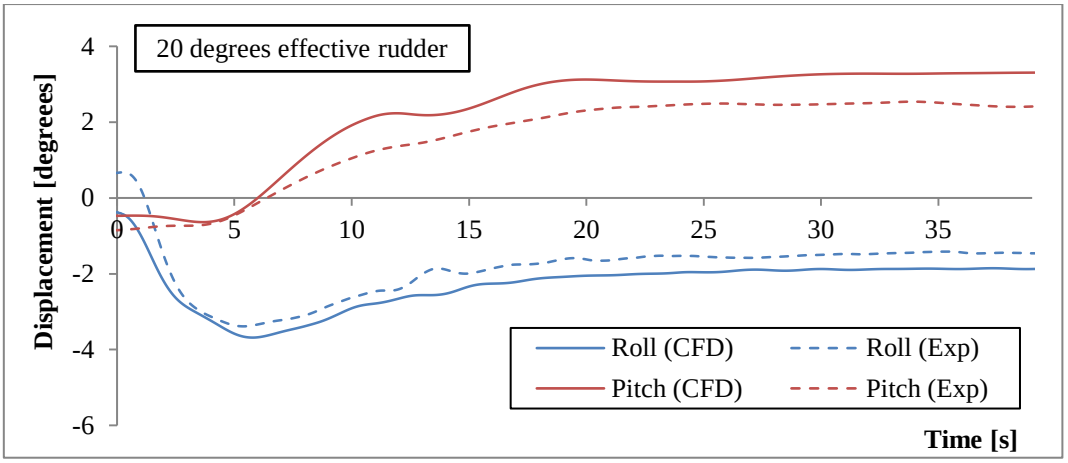

(a)

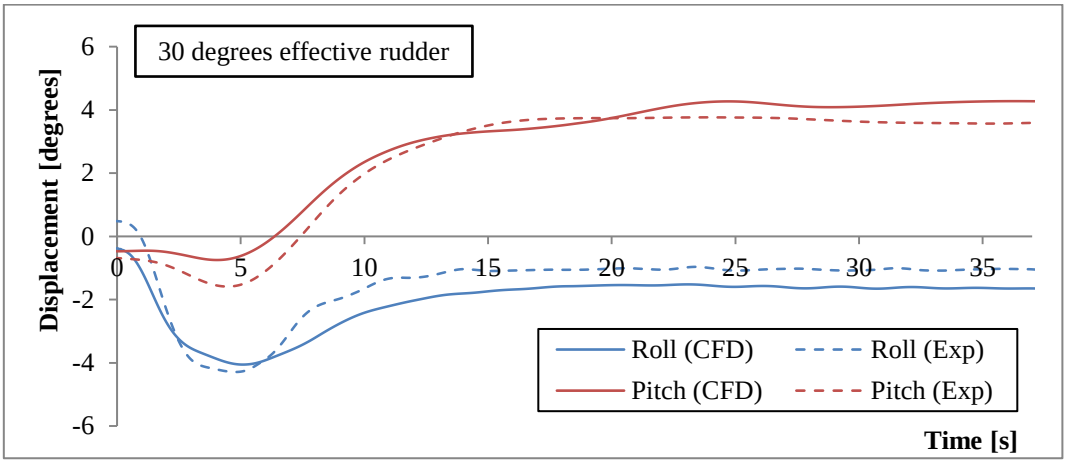

(b)

Figure 5-12: Time history of the roll (ϕ) and pitch (θ) angles for effective rudder angle of (a) 20 degrees and (b) 30 degrees steady turning manoeuvres at a forward speed of approximately 1.19 m/s.

The time series of the roll (*p*), pitch (*q*) and yaw (*r*) rates are shown in Figure 5-13. The CFD predictions converge to a fairly constant value and agree well with experimental data.

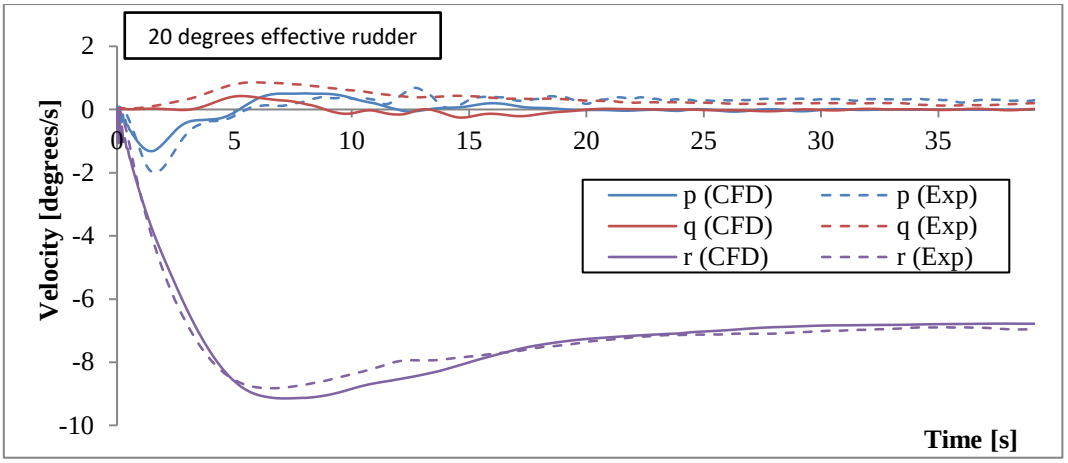

(a)

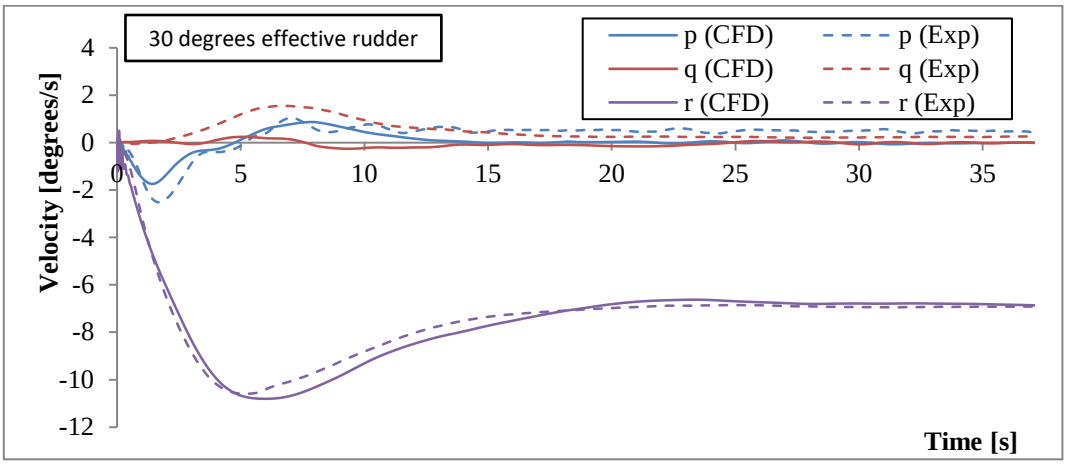

(b)

Figure 5-13: Time history of the angular velocities of the roll (*p*), pitch (*q*) and yaw (*r*) for effective rudder angle of (a) 20 degrees and (b) 30 degrees steady turning manoeuvres at a forward speed of approximately 1.19 m/s.

The angles of each control plane for effective rudder angle of 20 and 30 degrees turns are shown in Figure 5-14. While the effective rudder angles in the equation (5-5) were set to 20 and 30 degrees, the difference in the control plane angles between the CFD and experimental data were due to discrepancies in the calculated effective stern plane angles in the equation (5-6) which was affected by predictions of pitch angle and depth. Although the CFD predictions in the control plane angles are slightly different from the experimental measurements, the control planes are deemed to function correctly as the vehicle`s pitch angle and depth were maintained constant during the steady turn (shown in Figures 11 and 12).

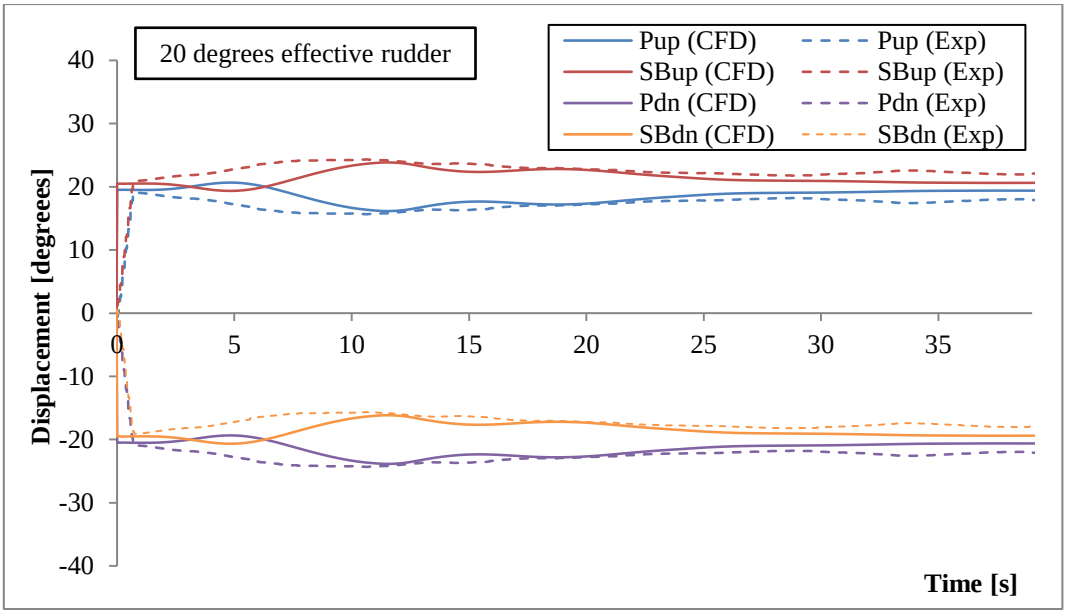

(a)

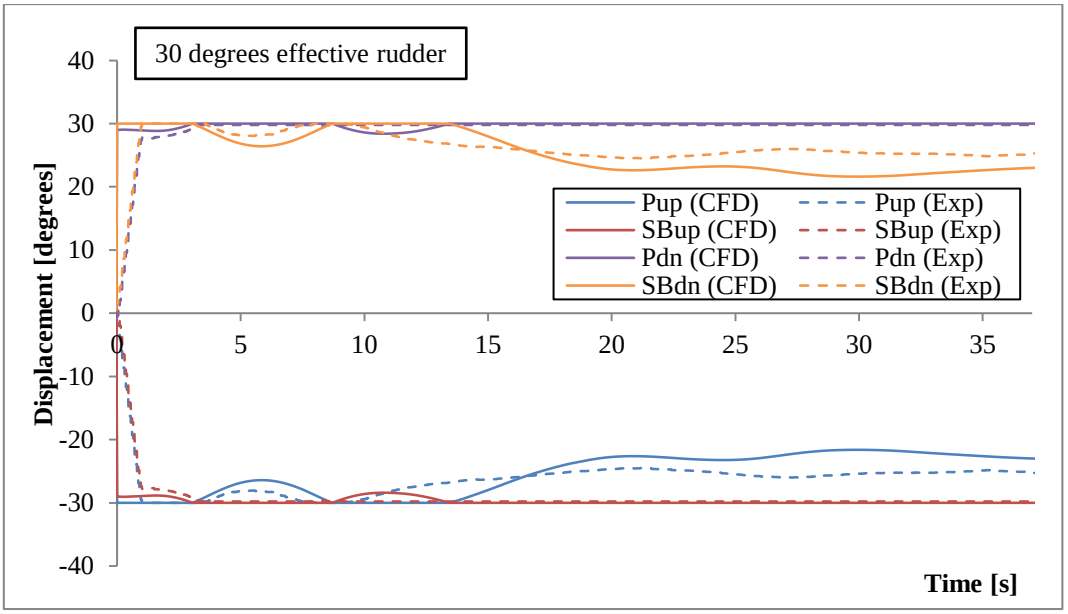

(b)

Figure 5-14: Time series of angle of the control planes for effective rudder angle of (a) 20 degrees and (b) 30 degrees steady turning manoeuvres at a forward speed of approximately 1.19 m/s.

5.4. Conclusions

This study investigated the capabilities of a CFD free running simulation model through the self-propelled BB2 undergoing straight line and steady turning manoeuvres in comparison to

experimental data. The simulations implemented an actuator disk propeller which prescribed the momentum sources based on the propeller characteristics obtained from a CFD captive self-propulsion test included in this study. The simulations also incorporated the dynamic deflection of the control planes in which the angles were commanded by an autopilot. The results showed that the full 6-DOF CFD manoeuvring model is able to predict a vehicle`s speed and manoeuvring characteristics (i.e. advance, transfer, tactical diameter and turning radius) that were in satisfactory agreement with experimental data, with a maximum error of 7.26 %.

Overall, this study shows that CFD is able to accurately simulate a free running test, which can be a cost-effective tool to complement and reduce the more expensive free running experimental work. The developed 6-DOF manoeuvring simulations will enable the designers to determine a vehicle’s manoeuvring characteristics, which is essential to design an adequate and accurate control system for the vehicle.

The capability of the present free running simulation is being extended to incorporate an actual propeller. This will allow for replicating the actual rotating flow that is able to address the discrepancies encountered with an actuator disk propeller. In addition, further work on the propulsion properties will be conducted by modelling the actual propeller operating in an oblique flow field, which should increase the accuracy of the results in the steady turning manoeuvring case.

PART 5B: Zig-zag manoeuvre

This sub-chapter presents preliminary simulation results for the BB2 model scale submarine undergoing a 20/20 horizontal plane zig-zag manoeuvre. The results are compared against experimental measurements provided by MARIN (Overpelt et al., 2015). The simulation employs the same geometry, grid and simulation settings as discussed in Part 5A. This work is currently being finalised and will be published in near future.

5.5. Introduction

This section outlines the preliminary results for a free running simulation of the BB2 model scale submarine undergoing a 20/20 horizontal plane zig-zag manoeuvre (as defined in ITTC, 2011a) at approximately 1.19 m/s with a constant propeller rotation. Validation is carried out by comparing the simulation results against the experimental measurements obtained at MARIN (Overpelt et al., 2015). This simulation and validation work is currently being finalised and will be published in near future.

5.6. Methodology

The CFD free running simulation utilised the same grid and simulation settings as described in Part 5A, for the BB2 model-scale submarine (Overpelt et al., 2015) operating with movable aft control planes and a body force propeller (see Figure 5-15). For the 20/20 horizontal plane zig-zag manoeuvre, the effective rudder angle (δ_r) is initially set to -20 degrees and held steady until the vehicle`s yaw heading angle become -20 degrees (see Figure 5-16). The rudder angle is then changed to +20 degrees and the manoeuvre repeated. The depth and pitch angle are maintained during the manoeuvre by the stern planes with the sail planes kept at zero angle.

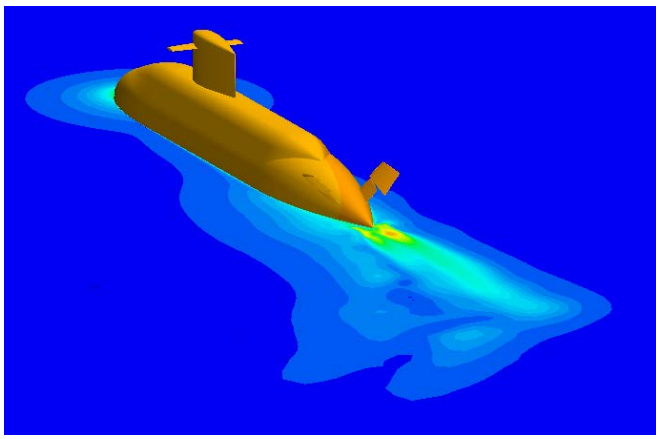

Figure 5-15: Free running CFD simulation of the BB2 model scale submarine undergoing a 20/20 zig-zag manoeuvre with movable aft control planes and a body force propeller. The horizontal slice plane shows the velocity field.

5.7. Results

Figure 5-16 shows the time histories of the vehicle`s roll (ϕ), pitch (θ), yaw (ψ) and the prescribed effective rudder angles for the 20/20 zig-zag manoeuvre. The CFD results in Figure 5-16 (a) are qualitatively good compared to the experiment measurements, with the errors of the yaw angle overshoot and phase differences well within 10%. These errors are attributed to the control plane displacement rate limiter of 30.46 degrees/s in the experimental setup that was not replicated in the CFD simulation. This is currently being implemented in the CFD model, which should improve the comparison between the CFD and experimental results.

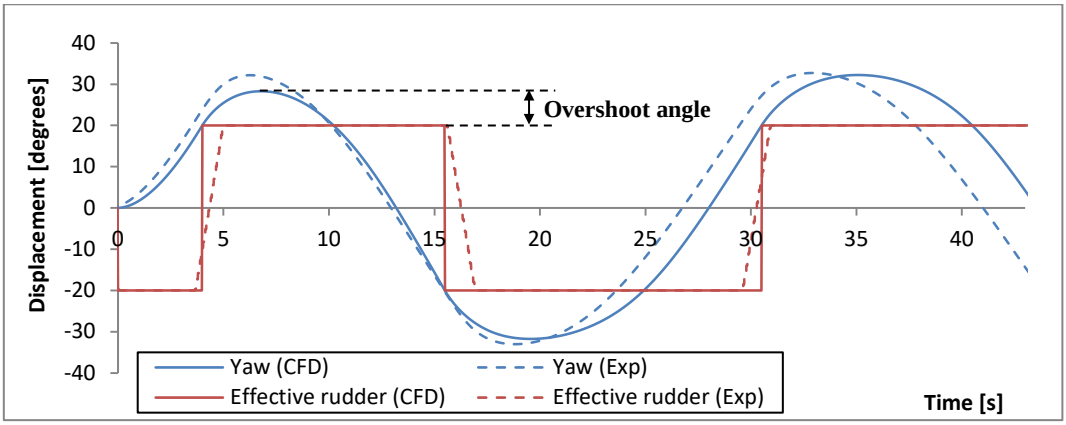

(a)

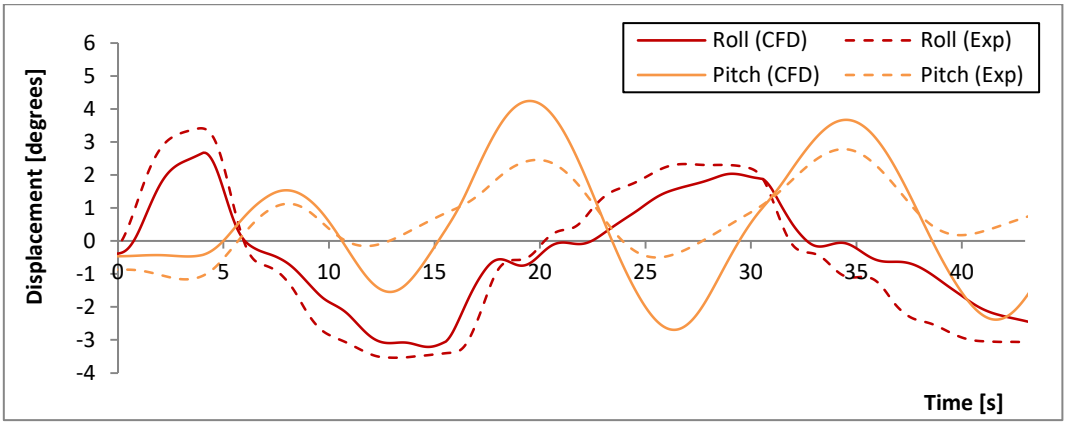

(b)

Figure 5-16: Time series results for a 20/20 zig-zag manoeuvre of the BB2 model scale submarine executed at a forward speed of approximately 1.19 m/s: (a) yaw and effective rudder angles; and (b) roll and pitch angles.

Figure 5-16 (b) shows that the general trend of the roll and pitch angles are well captured by the CFD in comparison to the experimental data, although the errors of the roll and pitch angles

are found to be a maximum of 2.5 degrees. The errors are attributed to the exclusion of moving sail planes for vertical control in the CFD simulation, as the experiment utilised both the sail planes and aft control surfaces for vertical control. The vehicle showed a bow up attitude when the vehicle`s yaw is at the maximum overshoot angles due to the presence of the sail that causes an out-of-plane downward force on the vehicle`s stern region (Leong et al., 2016). Further simulations are currently being carried out with the inclusion of moving sail planes to replicate the experimental setup.

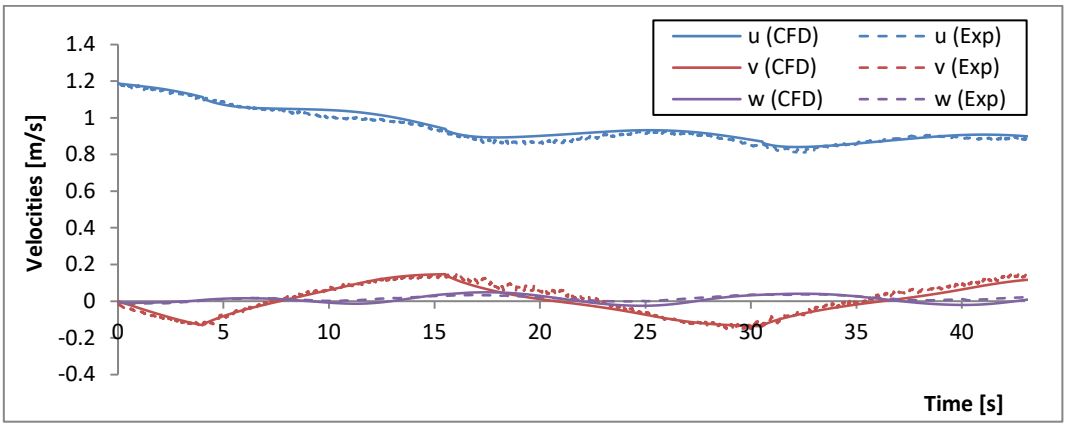

(a)

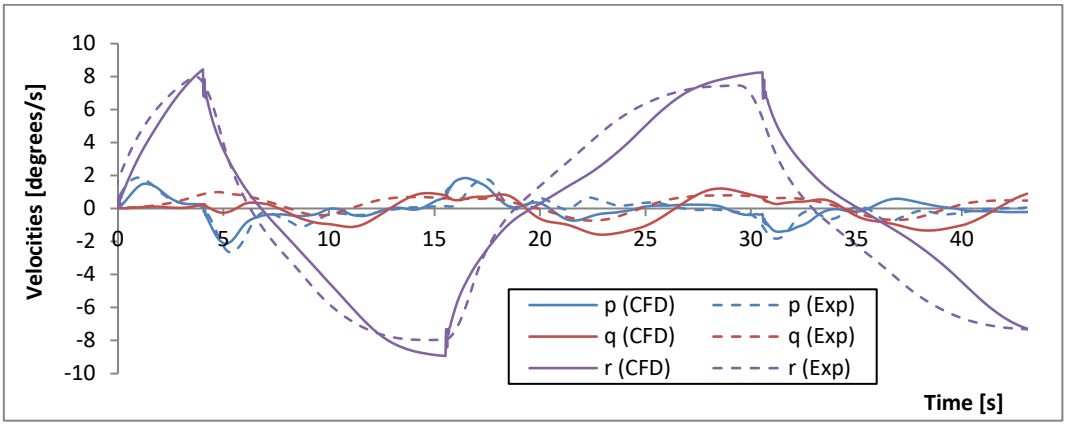

(b)

Figure 5-17: Time series results for a 20/20 zig-zag manoeuvre of the BB2 model scale submarine executed at a forward speed of approximately 1.19 m/s: (a) linear (*u*, *v* and *w*) velocities; and (b) angular (*p*, *q* and *r*) velocities.

The time series of linear (*u*, *v* and *w*) and angular velocities (*p*, *q* and *r*) are shown in Figure 5-17. It is observed that the general trends in the CFD predictions were in good agreement with the experimental measurements for the linear velocities. A more notable variance in the angular

velocities was observe which should improve with the inclusion of the maximum control plane rate limiter and the movable sail planes introduced into the new CFD simulation model.

5.8. Conclusions and Further Work

This section presented the preliminary CFD predictions for a 20/20 horizontal plane zig-zag manoeuvre for the BB2 model scale submarine and its comparison against available experimental data (Overpelt et al., 2015). The CFD predictions are generally in good agreement with the experimental measurements, although some angular parameters do exhibit some differences. These are attributed to the exclusion of the control plane displacement rate limiter and the movable sail planes in the CFD simulation model. These are currently being included and additional horizontal and vertical plane zig-zag manoeuvres are being carried out. These will be published in the near future.

[Page intentionally left blank]

Chapter 6: Summary, Conclusions and Future work

This chapter presents the overall summary and conclusions on the findings in this project, followed by recommendations to provide guidance for future work.

6.1. Summary

This thesis presents an investigation into Computational Fluid Dynamics (CFD) as a System-Based Design (SBD) tool to develop Six-DOF (6-DOF) free running simulation manoeuvring models of a fully appended underwater vehicle. This simulations enable the designers to determine a vehicle's manoeuvring characteristics for control system design and its safe operational limits. A review of the literature showed that free running tests of underwater vehicles have often been carried out experimentally using physical models operated in controlled environments, which has a number of limitations due to costs and the need for specialised equipment and facilities. With increasing capabilities in CFD and High Performance Computing (HPC), CFD-based free running simulations are now well suited to supplement experimental studies. However, the required capabilities of the simulations, including 6-DOF motion and action of the propeller and control planes, have yet to be established and validated, which forms the motivation of this project.

The selected underwater vehicles for the simulation work was the fully appended DST/MARIN generic submarine hull form BB2, with the physical free running model testing carried out and published by MARIN (Overpelt et al., 2015). The vehicles has also undergone numerous simulations and captive model experiments to identify its hydrodynamics characteristics in a number of configurations, ranging from bare hull to its fully appended configuration. The modelling was performed using two commercial CFD software packages: ANSYS-CFX and Star CCM+. The project initially utilised ANSYS-CFX but switched to Star CCM+ owing to limitations of the former in modelling the 6-DOF fully appended free running simulation. At the time of this change, ANSYS-CFX did not have a built-in capability of defining a local coordinate system for individually moving components (i.e. hull, propeller, and control planes). The global coordinate was set as a default and could not be altered. This issue was resolved with Star CCM+ that enabled the user to specify multiple local coordinates. This was essential to define motion of individual components moving independently of the vehicle`s motion. The various coordinates were fixed to specified locations on the vehicle. Another limitation was that ANSYS-CFX v14.5 offered only two dynamic gridding techniques (i.e. immersed solid and re-meshing) that were determined to be inappropriate for the 6-DOF free running model. The immersed solid method was unable to accurately predict forces on an object owing to its inability to accurately account for the boundary layer. The re-meshing method was

computationally extensive owing to continuous mesh updates. These grid technique drawbacks were resolved by using the overset gridding method available in Star CCM+. Note that the simulations conducted in Chapters 2 to 4 were performed using the Baseline Reynolds stress model (ANSYS, 2012), whilst those in Chapter 5 were based on the Elliptic blending Reynolds stress model (CD-adapco, 2015).

This project adopted a build-up approach to first investigate the hydrodynamics of an underwater vehicle's individual component. The work commenced investigating bare hull and different propeller models, such as a rotating propeller and a body force (actuator disk) model. The final 6-DOF simulation model consisted of the fully appended vehicle configuration that included the hull with casing, forward and aft control surfaces, and the propeller.

Initially a bare hull model undergoing prescribed pure sway and pure yaw motions was numerically simulated and validated using experimental hydrodynamic force and moment measurements on the hull obtained through Horizontal Planar Motion Mechanism (HPMM) work at the Australian Maritime College Towing Tank (AMCTT). This established the appropriate CFD methodology to accurately predict the hydrodynamic loads, which forms the foundation for the free running simulation model.

The propeller modelling commenced with the CFD simulation of an open water propeller validated against data from the Australian Maritime College Cavitation Research Laboratory (AMC CRL) to examine its hydrodynamic characteristics. The CFD model was able to successfully predict the global field quantities at various speeds of advance. The developed methodology was then adopted in the captive self-propulsion test of the underwater vehicle that provided the propeller propulsion properties for the body force propeller used in the free running simulations.

The capability of CFD free running simulations was examined through the motion predictions of the coupled flow and Rigid Body Dynamics (RBD) solver simulations. The simulations implemented two propulsion types: a prescribed thrust force and a body force propeller model using an actuator disk. The thrust force were first imposed on two bare hulls (i.e. an axisymmetric prolate spheroid and the SUBOFF generic submarine geometry) undergoing

straight line manoeuvres. This was followed by the addition of an actuator disk to a fully appended SUBOFF hull.

Finally a number of 6-DOF manoeuvring simulations were performed for the fully appended BB2 submarine hull form undergoing three generic manoeuvring tests (i.e. straight line, steady turning, and zig-zag manoeuvres) with an actuator disk propulsion model and movable control planes commanded by an autopilot. The dynamic deflection of the control planes was realised using an overset grid technique. The actuator disk propeller prescribed the rotational flow based on predetermined propulsion properties (i.e. thrust coefficient, K_T; torque coefficient, K_Q; and propeller efficiency, η) that were obtained from captive self-propulsion simulations using the actual propeller. The CFD simulations were validated against experimental measurements generated by MARIN from their physical free running model tests.

6.2. Conclusions

The main conclusions of this study on CFD as a system-based design tool to conduct 6-DOF free running manoeuvring simulations of a fully appended underwater vehicle are presented below:

- **Hydrodynamic loads on a fully submerged body:** Properly configured, CFD is clearly able to accurately predict hydrodynamic loads (forces and moments) on a fully submerged body undergoing steady-state and transient manoeuvres using URANS simulations, with good agreement against experimental data. This was established based on captive model tests on the SUBOFF submarine hull undergoing drift angle, pure sway and pure yaw manoeuvres, and the axisymmetric prolate spheroid body undergoing drift angle manoeuvres. However, CFD should not be used as an independent tool for hydrodynamic predictions, as results have shown that the accuracy is heavily dependent on the quality of the computational grid and the simulation model settings. Thus, it is essential that the CFD model is verified and validated to establish confidence in the predicted hydrodynamics for an underwater vehicle undergoing free running manoeuvres.

- **Dynamic motion of an underwater vehicle:** The combination of the moving domain and overset grid techniques has shown to be the most effective and efficient method in accurately describing the dynamic motion of an underwater vehicle. The moving domain approach overcomes the common restrictions of a grid deformation approach such as maintaining grid quality under deformation and the need for excessively large domains to capture the full motion of the vehicle. This essentially allows the vehicle to move without spatial restriction. However, the moving domain approach does not enable independent motions of multiple objects within the domain, thus requiring the inclusion of the overset grid technique for the movable control planes of the vehicle in the free running simulation.

- **Movable control planes using overset grid technique:** The overset grid technique has proven its capability to accurately and efficiently model the deflection of control planes on an moving underwater vehicle with a good agreement against experimental data. The overset grid technique is preferred to other options such as sliding and deforming grid for the free running simulation model. For deforming grid, it is difficult and expensive to maintain the grid quality during large deformations. In addition, unlike sliding grid, the overset grid technique can effectively handle the intersection between rotating and stationary surfaces within the tolerance of the existing grid by allowing a rotating surface/domain to pass through a stationary surface.

- **Propulsor:** The body force propeller (actuator disk) is the preferred propulsor option in comparison to a physically rotating propeller for the CFD simulation of a free running model. The body force propeller option significantly reduces computational time against the rotating propeller option, that latter requiring large computational resources and lengthy simulation time due to the fine spatial and temporal resolutions to resolve its flow field and revolutions. However, it is noted that the body force propeller model requires pre-determined propeller performance characteristics, which may require either CFD or experimental work to quantify the characteristics. The body force propeller has performed well for the manoeuvring trials (i.e. straight line, steady turning and zig-zag manoeuvres) with good agreement against experimental data.

- **Motion response of the vehicle in 1-DOF:** The free running simulation model developed for the 1-DOF straight line manoeuvre is clearly able to simulate an underwater vehicle moving in response to external forces. However, it is important to note that the 1-DOF model is limited in representing the actual behaviour of the vehicle undergoing a straight line manoeuvre. This is attributed to a non-axisymmetric body due to the presence of the casing, sail and sail planes; and the absence of control plane action to compensate for the vehicle`s roll, pitch, yaw, heave and sway variations in order to maintain its trajectory (as shown in both the numerical and experimental 6-DOF results).

- **Motion response of the vehicle in 6-DOF:** The 6-DOF CFD URANS free running simulation model with movable control planes and a body force propeller developed in this study clearly proved its ability to accurately replicate the free running experiments conducted by MARIN . The following conclusions are based on the three 6-DOF manoeuvring trials investigated, i.e. straight line, steady turning and zig-zag manoeuvres.

    - ***Straight line manoeuvre:*** The simulation results demonstrated the feasibility of providing a thrust force corresponding to the prescribed revolution speeds in order to achieve the vehicle's target speeds. The CFD predictions of the rotational speed and thrust were in very good agreement with the experimental measurements, with differences of less than two percent. It was also shown that control planes commanded by the autopilot algorithm were able to maintain the straight line course during the manoeuvre.

    - ***Steady turning manoeuvre:*** The simulation model clearly demonstrated the feasibility of deflecting the control planes to carry out tuning manoeuvres while maintaining the vehicle's depth and pitch angle. The predictions showed good agreement with the experimental measurements, with a maximum discrepancy of less than eight percent for the manoeuvring characteristics (i.e. advance, trasfer, tactical diametre and turning radius). Overall, the time histories of the trajectories, velocities, thrust forces and angles of the individual control planes

proved that the 6-DOF manoeuvring model provides manoeuvring predictions with good agreement against the experimental measurements.

- ***Zig-zag manoeuvre:*** The preliminary comparisons between CFD results and experimental measurements have shown that the free running simulation model is capable of predicting the vehicle`s behaviour observed in the experiments.

The work presented in the thesis has clearly shown that the CFD 6-DOF URANS free running simulation capability is a valuable tool that provides a cost effective method to obtain manoeuvring data in comparison to equivalent experimental testing. It also enables full scale data and flow visulisation (e.g. velocity and pressure fields) that is not always possible to obtain experimentally. The CFD results can be used to complement experimental free running programmes and indeed plan experimental campagnes that require significant resources and time.

6.3. Implications and Contribution to the Research Area

In this project, CFD and experimental studies were conducted to develop a validated 6-DOF CFD free running simulation model. This capability enables the 6-DOF simulation of an underwater vehicle moving in response to the actions of its control planes and propulsor, in order to examine its behaviour in a controlled environment. The simulation capability developed in this project will help designers to accurately determine the vehicle's manoeuvring characteristics for control system design, along with its manoeuvring efficiency. In addition, the accurate manoeuvring predictions of an underwater vehicle will contribute to enhancing the fidelity of establishing safe operating envelopes.

The work also included the validated CFD methodologies to represent the vehicle`s individual components, such as the hull and propeller, and the application of URANS to develop a free running simulation model. The presented methodologies will assist in further developing free running CFD simulations for the manoeuvring predictions of underwater vehicles undergoing various manoeuvres and operating conditions.

6.4. Further Work

The work presented in this thesis can be expanded to cover additional manoeuvring cases and operating conditions to provide data on the behaviour of the vehicles under those conditions. In addition, the use of a full scale submarine and a rotating propeller will enhance the fidelity of the simulations. Thus, the following recommendations for further work are presented:

- **The implementation of a rotating propeller in the 6-DOF free running simulations:** The present free running simulation model implemented an actuator disk in lieu of a rotating propeller for computational efficiency. As stated in Section 6.2, the pre-set propulsion properties were obtained from a CFD captive self-propulsion test under uniform fluid flow. This limits the accurate representation of the fluid flow field when operating in non-uniform conditions, such as within the boundary layer and wake of the vehicle. Although this limitation had little influence on the manoeuvring characteristics in the straight line, steady turning and zig-zag manoeuvres, it could be significant for extreme manoeuvres, such as emergency rising or crash back, which involves complex and highly transient flows. The implementation of an actual propeller will enable better representation of the flow characteristics around the propeller, thus improving accuracy. In addition, the modelling of the two propeller types within the 6-DOF simulation model will enable comparison of the two and possible improvements to the actuator disk model.

- **Further validation for more manoeuvring trials**: Further validation of CFD manoeuvring results against experimental measurements are suggested for more manoeuvring trials such as horizontal and vertical plane zig-zag manoeuvres. The preliminary validation of CFD results against experimental data showed a good agreement for a 20/20 horizontal plane zig-zag manoeuvre. Further simulations on additional horizontal and vertical plane zig-zag manoeuvres are currently being carried out.

- **Various operational conditions**: The present simulations were performed in fully submerged deep water conditions. The work can be further extended to various operational conditions such as near surface operations, near seabed/shallow water

environments, and operating in close proximity to other vehicles, especially those underway. Safe operation in these conditions becomes increasingly crucial due to a shift in focus to littoral operations and crowded surroundings (Bettle, 2013). When operating at near surface depths, a vehicle has a tendency to pitch bow down due to the presence of the free surface generating considerable suction force in the vehicle`s stern (Leong et al., 2016). Moreover, a vehicle passing in close proximity to another moving vehicle experiences hydrodynamic interaction effects which incurs rapid changes in the vehicle's acceleration. The results of the simulations will provide the necessary information to define the safe operating envelope for the vehicle, and detailed insight into the underlying physics of the vehicle's behaviour in that environment.

- **Full scale submarine simulations:** The present manoeuvring simulations were carried out using a model scale submarine to match the experimental setup. Further simulation using a full scale submarine is recommended to better represent actual conditions. In addition, the full scale manoeuvring simulations can complement the model scale experimental work that are often conducted at lower Reynolds numbers, producing a thicker boundary layer compared to the full scale condition. This can cause slower vehicle`s motion compared to full scale, affecting the velocities on the control planes during the manoeuvre.

[Page intentionally left blank]

References

Abkowitz, M. A. (1969). *Stability and Motion Control of Ocean Vehicles: Organization, Development, and Initial Notes of a Course of Instruction in the Subject*: MIT press. 0262510065.

Alin, N., Bensow, R., Fureby, C., Huuva, T., & Svennberg, U. (2010). Current capabilities of DES and LES for submarines at straight course. *Journal of Ship Research, 54*(3), 184-196.

ANSYS. (2009). CFX-Solver Manager User's Guide. *ANSYS CFX Release 12.1*, 42.

ANSYS. (2012). ANSYS CFX-solver theory guide. *ANSYS release 14.5*, 79-90, 94-100, 327-329.

Bettle, M. (2013). *Unsteady Computational Fluid Dynamics Simulations of Six Degrees-of-Freedom Submarine Manoeuvres.* (PhD), University of New Brunswick.

Bettle, M. C., Gerber, A. G., & Watt, G. D. (2009). Unsteady analysis of the six DOF motion of a buoyantly rising submarine. *Computers & Fluids, 38*(9), 1833-1849.

Blasius, H. (1907). *Grenzschichten in Flüssigkeiten mit kleiner Reibung. Inaugural-Dissertation... von H. Blasius*: Druck von BG Teubner.

Burcher, R., & Rydill, L. J. (1995). *Concepts in submarine design*: Cambridge University Press. 052155926X.

Carlton, J. (2012). *Marine propellers and propulsion*: Butterworth-Heinemann. 0080971245.

CD-adapco. (2015). STAR-CCM+ User Guide version 10.02.

Chase, N. (2012). *Simulations of the DARPA Suboff submarine including self-propulsion with the E1619 propeller.* (Master), University of Iowa.

Coe, R. G. (2013). *Improved Underwater Vehicle Control and Maneuvering Analysis with Computational Fluid Dynamics Simulations.* (PhD), Virginia Tech.

Cruz, N. A. (2011). *Autonomous Underwater Vehicles*: InTech. 9789533074320.

Doble, M. J., Forrest, A. L., Wadhams, P., & Laval, B. E. (2009). Through-ice AUV deployment: Operational and technical experience from two seasons of Arctic fieldwork. *Cold Regions Science and Technology, 56*(2), 90-97.

Dreyer, J. J., & Boger, D. A. (2010). *Validation of a free-swimming, guided multibody URANS simulation tools*. Paper presented at the 28th Symposium on Naval Hydrodynamics, Pasadena, USA, 12 - 17 September 2010.

Farrell, J. A., Pang, S., & Li, W. (2005). Chemical plume tracing via an autonomous underwater vehicle. *IEEE JOURNAL OF OCEANIC ENGINEERING, 30*(2), 428-442.

Feldman, J. (1979). *DTNSRDC Revised Standarrd Submarine Equations of Motion* (DTNSRDC/SPD-0393-09). Retrieved from http://www.dtic.mil/dtic/tr/fulltext/u2/a071804.pdf

Fossen, T. I. (1994). *Guidance and Control of Ocean Vehicles*. Chichester, UK: John Wiley and Sons Ltd. 9780471941132.

German, C., Connelly, D., Prien, R., Yoerger, D., Jakuba, M., Bradley, A., . . . Langmuir, C. (2004). *New techniques for hydrothermal exploration: In situ chemical sensors on AUVs-Preliminary results from the Lau Basin*. Paper presented at the American Geophysical Union Fall Meeting, San Francisco, USA, 13-17 December 2004.

Gertler, M., & Hagen, G. R. (1967). *Standard equations of motion for submarine simulation* (NSRDC-2510). Retrieved from http://www.dtic.mil/dtic/tr/fulltext/u2/653861.pdf

Godderidge, B., Phillips, A. B., Lewis, S. G., Turnock, S. R., Hudson, D. A., & Tan, M. (2008). *The simulation of free surface flows with Computational Fluid Dynamics*. Paper presented at the Ansys UK User Conference: Inspiring Engineering, Oxford, UK, 29-30 October 2008.

Goldstein, S. (1929). On the vortex theory of screw propellers. *Proceedings of the Royal Society of London. Series A, Containing Papers of a Mathematical and Physical Character, 123*(792), 440-465.

Grasmueck, M., Eberli, G. P., Viggiano, D. A., Correa, T., Rathwell, G., & Luo, J. (2006). Autonomous underwater vehicle (AUV) mapping reveals coral mound distribution, morphology, and oceanography in deep water of the Straits of Florida. *Geophysical Research Letters, 33*(23).

Groves, N. C., Huang, T. T., & Chang, M. S. (1989). *Geometric Characteristics of DARPA Suboff Models:(DTRC Model Nos. 5470 and 5471)* (DTRC/SHD-1298-01). Retrieved from http://www.dtic.mil/dtic/tr/fulltext/u2/a210642.pdf

Guilmineau, E., Deng, G. B., Leroyer, A., Queutey, P., Visonneau, M., & Wackers, J. (2014). *Wake simulatoin of a marine propeller*. Paper presented at the 11th World Congress on computational mechanics, Barcelona, Spain, 20-25 July 2014.

Hally, D. (2009). *Grid dependence of RANS codes for flows past propeller blade sections* (DRDC Atlantic TM 2008-262). Retrieved from http://www.dtic.mil/dtic/tr/fulltext/u2/a514605.pdf

Hama, F. R. (1957). An Effective Tripping Device. *Journal of the Aeronautical Sciences, 24*(3), 236-237.

Hough, G., & Ordway, D. (1964). *The generalized actuator disk* (TAR-TR 6401). Retrieved from http://www.dtic.mil/dtic/tr/fulltext/u2/433976.pdf

Issac, M. T., Adams, S., He, M., Bose, N., Williams, C. D., Bachmayer, R., & Crees, T. (2007). *Manoeuvring experiments using the MUN Explorer AUV.* Paper presented at the 2007 Symposium on Underwater Technology and Workshop on Scientific Use of Submarine Cables and Related Technologies, Tokyo, Japan, 17-20 April 2007.

Itard, X. (1999). *Recovery procedure in case of flooding.* Paper presented at the Warship '99 International Symposium, London, UK, 16 June 1999.

ITTC. (2002a). *ITTC – Recommended Procedures: Full Scale Measurements Manoeuvrability Full Scale Manoeuvring Trials Procedure* Paper presented at the 23th Int Towing Tank Conference, Venice, Italy, 8-14 September 2002.

ITTC. (2002b). *Testing and Extrapolation Methods Resistance Uncertainty Analysis*. Paper presented at the 23th Int Towing Tank Conference, Venice, Italy, 8-14 September 2002.

ITTC. (2011a). *Final Report and Recommendations to the 26th ITTC.* Paper presented at the 26th Int Towing Tank Conference, Rio de Janeiro, Brazil, 28 August - 3 September 2011.

ITTC. (2011b). *Recommended Procedures and Guidelines: Model Manufacture Ship Models.* Paper presented at the 26th Int Towing Tank Conference, Rio de Janeiro, Brazil, 28 August - 3 September 2011.

ITTC. (2014). *ITTC Symbols and Terminology List*. Paper presented at the 27th Int Towing Tank Conference, Copenhagen, Denmark, 31 August - 5 September 2014.

Jagadeesh, P., Murali, K., & Idichandy, V. G. (2009). Experimental investigation of hydrodynamic force coefficients over AUV hull form. *Ocean Engineering, 36*(1), 113-118.

Joubert, P. N. (2006). *Some Aspects of Submarine Design: Part 2. Shape of submarine 2026* (DSTO-TR-1920). Retrieved from http://dspace.dsto.defence.gov.au/dspace/bitstream/1947/8027/1/DSTO-TR-1920.PR.pdf

Joung, T.-h., Sammut, K., & He, F. (2010). *A CFD (Computer Fluid Dynamics) analysis based design method for an autonomous underwater vehicle ducted propeller*. Paper

presented at the The Twentieth International Offshore and Polar Engineering Conference, Beijing, China, 20-25 June 2010.

Jun, B., Park, J., Lee, F., Lee, P., Lee, C., Kim, K., . . . Oh, J. (2009). Development of the AUV 'ISiMI' and a free running test in an Ocean Engineering Basin. *Ocean Engineering, 36*(1), 2-14.

Kerkvliet, M. (2013). *Influence on the numerical uncertainty of a generic submarine model by changing the wall-normal distribution of the wall-bounded grid cells.* Paper presented at the 16th Numerical Towing Tank Symposium (NuTTS), Müllheim, Germany, 2-4 September 2013.

Kim, H., Leong, Z. Q., Ranmuthugala, D., Chin, C., & Forrest, A. (2015a). *Free running simulation of an Autonomous Underwater Vehicle undergoing a straight line manoeuvre via Computational Fluid Dynamics.* Paper presented at the Pacific International Maritime Conference, Sydney, Australia, 6-8 October 2015.

Kim, H., Leong, Z. Q., Ranmuthugala, D., & Forrest, A. (2015b). Simulation and Validation of an AUV in Variable Accelerations. *International Journal of Offshore and Polar Engineering, 25*(01), 35-44.

Kim, H., Ranmuthugala, D., Leong, Z. Q., & Chin, C. (2018). Six-DOF simulations of an underwater vehicle undergoing straight line and steady turning manoeuvres. *Ocean Engineering, 150*, 102-112.

Leong, Z. Q., Piccolin, S., Desjuzeur, M., Ranmuthugala, D., & Renilson, M. (2016). *Evaluation of the Out-of-Plane loads on a submarine undergoing a steady turn.* Paper presented at the 20th Australasian Fluid Mechanics Conference, Perth, Australia, 5-8 December 2016.

Lewis, E. V. (1988). *Principles of Naval Architecture - Resistance, Propulsion and Vibration* (Vol. 2). Jersey City: SNAME. 9780939773015.

Liu, H.-L., & Huang, T. T. (1998). *Summary of DARPA SUBOFF experimental program data* (CRDKNSWC/HD-1298-11). Retrieved from http://www.dtic.mil/dtic/tr/fulltext/u2/a359226.pdf

Lu, N. X., Svennberg, U., Bark, G., & Bensow, R. (2012). *Numerical simulations of the cavitating flow on a marine propeller.* Paper presented at the 8th International Symposium on Cavitation, Singapore, 13 - 16 August 2012.

Luo, H., Sharov, D., Baum, J. D., & Loehner, R. (2001). On the computation of compressible turbulent flows on unstructured grids. *International Journal of Computational Fluid Dynamics, 14*(4), 253-270.

Malik, S., & Guang, P. (2013). Transient Numerical Simulations for Hydrodynamic Derivatives Predictions of an Axisymmetric Submersible Vehicle. *Research Journal of Applied Sciences, Engineering and Technology, 5*(21), 5003-5011.

McDonald, H., & Whitfield, D. (1996). *Self-propelled maneuvering underwater vehicles.* Paper presented at the The 21st Symposium on Naval Hydrodynamics, Trondheim, Norway, 24–28 June 1996.

Morgut, M., & Nobile, E. (2012). Influence of grid type and turbulence model on the numerical prediction of the flow around marine propellers working in uniform inflow. *Ocean Engineering, 42*, 26-34.

Navy, U. (2004). The navy unmanned undersea vehicle (UUV) master plan. *US Navy,. 9*, 90.

Neulist, D. (2011). *Experimental investigation into the hydrodynamic characteristics of a submarine operating near the free surface.* (Bachelor of Engineering, Final Year Thesis (Honours)), Australian Maritime College, Launceston.

Norrison, D., Sidebottom, W., Anderson, B., Petterson, K., & Fureby, C. (2016). *Numerical Study of a Self-Propelled Conventional Submarine*. Paper presented at the 31st Symposium on Naval Hydrodynamics, Monterey, USA, 11-16 September 2016.

Overpelt, B., Nienhuis, B., & Anderson, B. (2015). *Free Running Manoeuvring Model Tests On A Modern Generic SSK Class Submarine (BB2).* Paper presented at the Pacific International Maritime Conference, Sydney, Australia, 6-8 October 2015.

Pankajakshan, R., Remotigue, M. G., Taylor, L. K., Jiang, M., Briley, W. R., & Whitfield, D. L. (2002). *Validation of Control-Surface Induced Submarine Manoeuvring Simulations using UNCLE*. Paper presented at the 24th Symposium on Naval Hydrodynamics, Fukuoka, Japan, 8-13 July 2002.

Paul, G., Joubert, P. N., & Chong, M. (2004). *Flow over a Body of Revolution in a Steady Turn* (DSTO-TR-1591). Retrieved from http://dspace.dsto.defence.gov.au/dspace/bitstream/1947/4398/1/DSTO-TR-1591.pdf

Phillips, A. (2010). *Simulations of a self propelled autonomous underwater vehicle.* (PhD), University of Southampton.

Phillips, A., Turnock, S., & Furlong, M. (2008). *Comparisons of CFD simulations and in-service data for the self propelled performance of an Autonomous Underwater Vehicle*.

Paper presented at the 27th Symposium on Naval Hydrodynamics, Seoul, Korea, 5-10 October 2008.

Prandtl, L. (1904). Uber Flussigkeits bewegung bei sehr kleiner Reibung. *Verhaldlg III Int. Math. Kong*, 484-491.

Prandtl, L. (1935). The mechanics of viscous fluids. *Aerodynamic theory, 3*(344), 208.

Ross, A., Perez, T., & Fossen, T. I. (2007). A novel manoeuvering model based on low-aspect-ratio lift theory and Lagrangian mechanics. *IFAC Proceedings Volumes, 40*(17), 229-234.

Sakamoto, N., Carrica, P. M., & Stern, F. (2012). URANS simulations of static and dynamic maneuvering for surface combatant: Part 1. Verification and validation for forces, moment, and hydrodynamic derivatives. *Journal of Marine Science and Technology (Japan), 17*(4), 422-445.

Sariel, S., Balch, T., & Stack, J. (2006). *Distributed multi-auv coordination in naval mine countermeasure mrrrrissions* (Tech Report GIT-GVU-06-04). Retrieved from https://smartech.gatech.edu/bitstream/handle/1853/8722/06-04.pdf

Song, B.-w., Wang, Y.-j., & Tian, W.-l. (2015). Open water performance comparison between hub-type and hubless rim driven thrusters based on CFD method. *Ocean Engineering, 103*, 55-63.

Steel, S. V. (2010). *Investigation into the effect of wave making on a submarine approaching the surface.* (Bachelor of Engineering, Final Year Thesis (Honours)), Australian Maritime College, Launceston.

Stern, F., Yang, J., Wang, Z., Sadat-Hosseini, H., Mousaviraad, M., Bhushan, S., & Xing, T. (2013). Computational ship hydrodynamics: Nowadays and way forward. *International Shipbuilding Progress, 60*(1), 3-105.

Tyagi, A., & Sen, D. (2006). Calculation of transverse hydrodynamic coefficients using computational fluid dynamic approach. *Ocean Engineering, 33*(5), 798-809.

Watt, G. D. (2007). *Modelling and simulating unsteady six degrees-of-freedom submarine rising maneuvers* (DRDC Atlantic TR 2007-008). Retrieved from http://www.dtic.mil/dtic/tr/fulltext/u2/1005166.pdf

Werner, S., Pistidda, A., Larsson, L., & Regnström, B. (2007). Computational fluid dynamics validation for a fin/bulb/winglet keel configuration. *Journal of Ship Research, 51*(4), 343-358.

Wetzel, T. G. (1996). *Unsteady Flow Over a 6:1 Prolate Spheroid.* (PhD), Virginia Tech, Blacksburg.

White, F. M. (2011). *Fluid mechanics*: McGraw-Hill, New York. 9780071311212.

Wilson-Haffenden, S. (2009). *An Investigation into the Wave Making Resistance of a Submarine Travelling Below the Free Surface.* (Bachelor of Engineering, Final Year Thesis (Honours)), Australian Maritime College, Launceston.

Zhang, H., Xu, Y.-r., & Cai, H.-p. (2010). Using CFD Software to Calculate Hydrodynamic Coefficients. *Journal of Marine Science and Application, 9*(2), 149-155.

Zierke, W. C., Boger, D. A., Davoudzadeh, F., & McDonald, H. (1997). *A Physics-Based Means of Computing the Flow Around a Maneuvering Underwater Vehicle* (TR 97-002). Retrieved from http://www.dtic.mil/dtic/tr/fulltext/u2/a322316.pdf

[Page intentionally left blank]

APPENDIX I: Dynamic Grid Techniques

The following dynamic meshing techniques coupled with Rigid Body Solver (RBS) were initially investigated to realise the vehicle's motion in response to the external forces.

- MDM;
- Immersed Solids Method (ISM); and
- Re-Meshing Method (RMM).

The capabilities of these methods were examined using the spheroid undergoing straight line manoeuvres by various axial forces. These forces were firstly predicted at different axial speeds and used as an external input force to enforce the rigid body (see Table I-1).

Table I-1: Prediction of the axial forces at various axial speeds.

Axial speed [m/s]	Axial force [N]
0.500	0.646
1.000	2.325
1.200	3.251
2.000	8.455
2.500	12.851

- **MDM vs ISM**

Figure I-1 shows the time history of the predicted axial forces acting on the body against external input forces, adopting the coupled RBD solver with MDM and ISM. It shows that the axial forces predicted by MDM coupled with RBD were almost identical to the external input forces. However, ISM interfaced with RBD provided up to 10% less axial force prediction at 2.500 m/s than the external input forces. Moreover, the instability of the predictions was found due to the absence of the accurate near wall modelling.

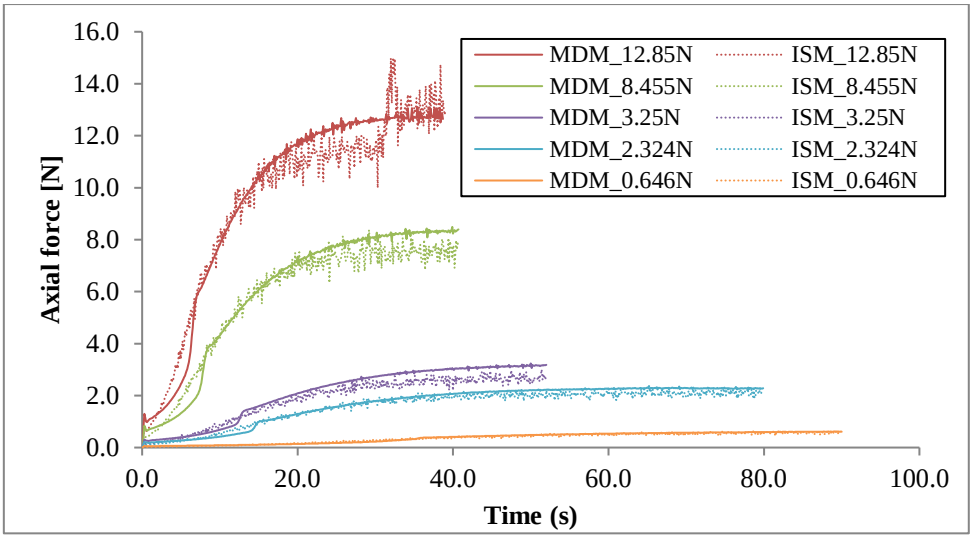

Figure I-1: Time history of the axial force predictions by coupling of the 6-DOF RBS with MDM and ISM (the forces in the legend represents the external input forces).

Figure I-2 shows the time series of the axial speeds of the body with respect to the external input forces. Similar to the previous results, ISM under predicted the speed by up to 16% at 2.500 m/s mainly due to inadequate near-wall modelling. MDM predictions on the other hand were very close to the corresponding speeds of the external input forces.

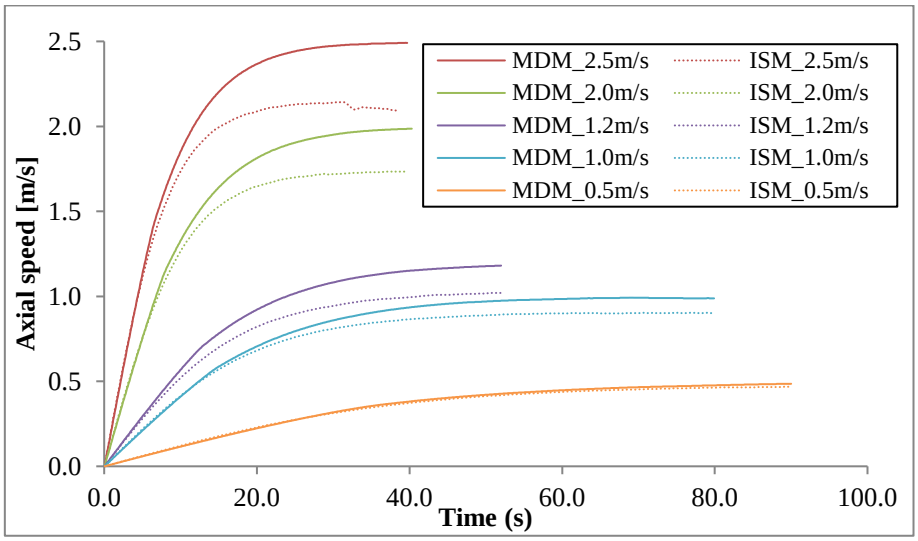

Figure I-2: Time history of the axial speed predictions by coupling of the 6-DOF RBS with MDM and ISM (the speeds in the legend represents the corresponding speed to the external input force).

Consequently, it was found that MDM is far superior for modelling the simulation of the body moving in response to external forces, compared to ISM. The inadequate near wall modelling has shown to provide poor prediction of axial forces and speeds at the higher external input forces. Although the ISM provided less accurate results, this method can be a worthwhile solution for a case where accurate mesh generation is difficult due to the complexity of the geometry.

- **MDM vs RMM**

RMM can be implemented to improve the mesh quality (e.g. orthogonality, expansion, and aspect ratio) during the simulation run. The capability of RMM in the present study was examined by defining the re-meshing criteria (i.e. minimum orthogonality angle >10 degrees). In order to demonstrate the effect of RMM, the comparison of the results between MDM and RMM were carried out. Figure I-3 shows the time series of the axial forces predictions acting on the body against the external input forces by MDM and RMM. Both methods enabled predicting the axial forces identical to the applied input forces (i.e. 3.25 and 8.45 N). Note that the effective use of this method is necessary as RMM requires three times greater computational time than MDM in the current manoeuvring scenario (i.e. straight line manoeuvre). With its advantage of controlling the level of the allowable mesh qualities, RMM can be an effective option for a simulation where large mesh deformation occurs.

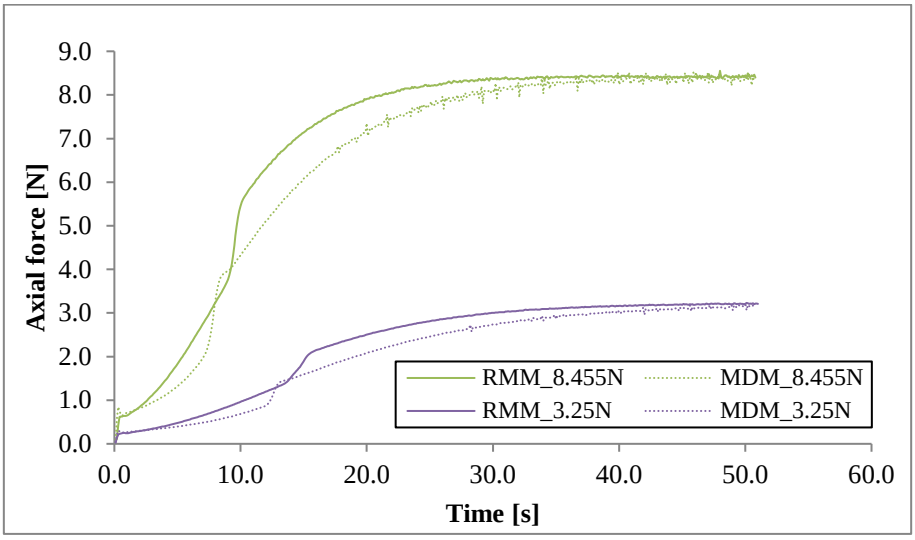

Figure I-3: Time history of axial force predictions at the different external input force, by adopting MDM and RMM.

APPENDIX II: Experimental Uncertainty Analysis

An experimental uncertainty analysis was complete using the methodology and guidelines by ITTC (2002b). The uncertainty for the single run and multiple run was calculated at 9.29% (≈ 10%) and 4.61% respectively. The former, 10%, was used as the experiment uncertainty threshold for comparison with CFD results for this study as it was the more conservative value of the two. Details of the uncertainty assessment are provided in Table II-1 below.

Table II-1: Experimental uncertainty analysis as per the methodology and guidelines by ITTC (2002b)

Model Particulars			
Definition	**Symbol**	**Value**	**Units**
Length overall submerged	L_{OS}	1.44	m
Diameter of hull	D	0.181	m
Wetted Surface Area - total	S	0.753	m^2
Wetted Surface Area - hull	S_{BH}	0.24	m^2
Wetted Surface Area- appendages	S_{APP}	0.032	m^2
Area Waterplane	A_{WP}	1.44	m^2
Displacement	V	0.181	m^3
Block Coefficient	C_B	0.628	-
Waterplane Area Coefficient	C_W	0.852	-
Wetted Surface Coefficient	C_S	3.491	-

Constant			
Definition	**Symbol**	**Value**	**Units**
Gravity	g	9.81	m/s^2
Density - reference	P_{ref}	1000	kg/m^3
Water Temp - test	t	18	deg
Water Density - test	ρ	997	kg/m^3
Pulse count	c	600	-
Time based circuitry	Δt	0.1	s
Carriage wheel diameter	D_W	0.555	m

Multiple Run Data Set					
Run No.	***U* [m/s]**	**R_x [gram]**	**R_x [N]**	**C_d**	**$(C_d - C_{d\,mean})^2$**
1	1.5	346.156	3.396	1.46E-03	2.71E-12
2	1.5	334.182	3.278	1.41E-03	1.73E-09

3	1.5	335.185	3.288	1.41E-03	1.44E-09
4	1.5	367.278	3.603	1.55E-03	6.08E-09
Mean	1.5	345.700	3.391	1.46E-03	-
Standard deviation					5.55E-05

Single Run Data Set				
Run No.	***U* [m/s]**	***R_x* [gram]**	***R_x* [N]**	***C_d***
1	1.5	334.182	3.278	0.00141

Measurement Accuracy and Bias			
Definition	**Symbol**	**Accuracy**	**Bias Limit**
Model Geometry			
Model Length	B_L	1.00E-03	2.00E-03
Carriage Speed			
Pulse Count	B_C	-	2.36E+00
Optical Encoder	B_{C1}	1.00E+00	1.00E+00
AD Converter 1	B_{C2}	1.50E+00	1.50E+00
AD Converter 2	B_{C3}	1.50E+00	1.50E+00
Voltage to Frequency Converter	B_{C4}	2.50E-01	2.50E-01
Wheel diameter	B_D	1.00E-03	1.00E-03
Time Base	$B_{\Delta t}$	1.03E-05	1.03E-05
Velocity	B_U	-	5.65E-03
Tank Water Temperature and Density			
Thermometer reading	B_T	5.00E-01	5.00E-01
Temp-density relationship	B_{P1}	9.20E-02	6.43E-02
Convert temp to density	B_{P2}	7.00E-02	7.00E-02
ITTC density assumption	B_{P3}	3.00E+00	3.00E+00
Density	B_P	-	3.00E+00
Resistance Measurement			
Accuracy of Calibration Weights	B_{RX1}	5.00E-05	5.66E-05
Mass/Voltage relationship SEE	B_{RX2}	3.07E-02	3.07E-02
Load cell misalignment	B_{RX3}	2.50E-01	1.08E-05
AD Converter	B_{RX4}	0.00E+00	0.00E+00
Inclination of model due to speed	B_{RX5}	2.50E-01	1.08E-05
Resistance	B_{RX}	-	3.07E-02
Coefficient of Total Resistance	B_{CT}	-	1.78E-05

Partial Derivatives

Definition	Symbol	Value
Partial Derivative - Resistance Coefficient		
$\frac{Rx}{0.5\rho U^2}(\frac{-1}{L^2})$	$\frac{\partial C_T}{\partial L}$	-7.03E-04
$\frac{Rx}{0.5\rho L^2}(\frac{-2}{U^3})$	$\frac{\partial C_T}{\partial U}$	-1.94E-03
$\frac{Rx}{0.5L^2U^2}(\frac{-1}{\rho^2})$	$\frac{\partial C_T}{\partial \rho}$	-1.46E-06
$\frac{1}{0.5\rho L^2U^2}$	$\frac{\partial C_T}{\partial R_x}$	4.30E-04
Partial Derivative - Velocity		
$\frac{\pi D}{8000\Delta t}$	$\frac{\partial U}{\partial c}$	7.11E-04
$\frac{c\pi}{8000\Delta t}$	$\frac{\partial U}{\partial D_W}$	2.36E+00
$\frac{c\pi D}{8000}(\frac{-1}{\Delta t^2})$	$\frac{\partial U}{\partial \Delta t}$	-4.26E+00
Partial Derivative - Density		
$\lvert 0.0552 - 0.0154t^2 + 0.000120t^2 \rvert$	$\left\lvert\frac{\partial \rho}{\partial t}\right\rvert$	-2.14E-01

Precision Limit (95% Confidence)		
Precision Limit	**Symbol**	**Value**
Multiple Sample Precision Limit	P_{CTM}	6.48E-05
Single Sample Precision Limit	P_{CTS}	1.30E-04

Total Uncertainty - Resistance Coefficient (95% Confidence)			
Uncertainty	**Symbol**	**Value**	**C_d [%]**
Multiple Sample Total Uncertainty	U_{CTM}	6.72E-05	4.61
Single Sample Total Uncertainty	U_{CTS}	1.31E-04	9.29